FFI-rapport 2015/00534

Modelling the elastic stiffness of nanocomposites using three-phase models

Tom Thorvaldsen

FFI Forsvarets forskningsinstitutt

Modelling the elastic stiffness of nanocomposites using three-phase models

Tom Thorvaldsen

Norwegian Defence Research Establishment (FFI)

15 June 2015

FFI-rapport 2015/00534

122701

P: ISBN 978-82-464-2552-8
E: ISBN 978-82-464-2553-5

Keywords

Elastisitet

Nanoteknologi

Matematiske modeller

Partikler

Approved by

Rune Lausund	Project Manager
Jon E. Skjervold	Director

English summary

This report describes mathematical modelling of the elastic stiffness of *nanocomposites*, which in this context is referred to as particles of nano-size included in a polymer matrix, i.e. particles with one dimension of nanometre size. The main motivation for this work was to establish mathematical models for calculating the elastic properties of different nanocomposites, which then can be included in a "model toolbox" for future applications and for improved understanding of this type of materials. In this study, it is assumed that micromechanics models and continuum mechanics theory can be applied in the modelling.

Another recent report describes two-phase models for calculation of the elastic stiffness for composites where the nanoparticles are perfectly dispersed in a polymer matrix. A general multi-phase Mori-Tanaka model was presented and implemented, in addition to more specialized expressions for composites with specific inclusion geometries and particle orientations. A perfect dispersion of nanoparticles in a matrix is, however, challenging to obtain. One therefore often ends up with a second inclusion phase with a different stiffness than the matrix and the particle. The second inclusion phase may be voids, with zero stiffness, or agglomerates of the primary particle. In both cases, the stiffness is believed to be lower than the matrix, giving a reduction in the overall composite stiffness.

In this report, different three-phase models found in the literature are described for investigating the effect on the composite elastic stiffness from a second inclusion phase. In particular, the general two-phase Mori-Tanaka model is extended to three phases. New models are also presented, being slightly modified and extended versions of those found in the literature. The model calculations are compared. The model results are also compared to experimental test results for two nanoparticle/epoxy systems.

As an overall conclusion, the model results for the three-phase models do agree with the experimental data to some extent. Including a second inclusion phase will reduce the overall stiffness of the composite, assuming that the stiffness of these inclusions is lower that the stiffness of the matrix. However, the effect from including a second inclusion phase in the modelling does not capture the high stiffness increase observed experimentally for low volume fractions; the three-phase models generally have a tendency to underestimate the elastic stiffness. An exception is the Paul model, but this model does not explicitly include the particle shape in the expressions, making it less flexible for various composites. Future studies should therefore consider other effects than those included in the current models. In particular, it is relevant to establish models that include a particle interphase, which may be modelled as a region surrounding the particles with different elastic properties compared to the neat matrix.

Sammendrag

Denne rapporten beskriver matematisk modellering av elastisk stivhet for nanokompositter, som i denne konteksten refererer til partikler av nanostørrelse som er inkludert i en polymermatrise, det vil si partikler der en av dimensjonene er i nanometer. Hovedmotivasjonen for dette arbeidet har vært å etablere matematiske modeller som kan benyttes for å beregne de elastiske egenskapene til ulike nanokompositter, som deretter kan inkluderes i en "modellverktøykasse" for fremtidige applikasjoner og for økt forståelse av denne typen materialer. Det er antatt at mikromekaniske modeller og kontinuummekanikk kan benyttes i modelleringen.

En annen nylig utgitt rapport beskriver to-fase-modeller for beregning av elastisk stivhet til kompositter der nanopartiklene er perfekt dispergert i en polymermatrise. En generell multi-fase Mori-Tanaka-modell ble presentert og implementert, i tillegg til mer spesialiserte uttrykk for analytiske uttrykk som er anvendbare for kompositter med gitte partikkelgeometrier og orientering. Perfekt dispersjon av nanopartikler i en matrise er derimot utfordrende å oppnå. Man ender derfor ofte opp med en ekstra inklusjonsfase som har en annen stivhet enn matrisen og primærpartikkelen. Den andre inklusjonsfasen kan være hulrom (gasslommer) med null stivhet, eller agglomerater av primærpartikkelen. I begge tilfeller er stivheten antatt å være lavere enn matrisens, noe som gir en lavere stivhet for kompositttet.

I denne rapporten er ulike tre-fase-modeller funnet i litteraturen beskrevet, med det formål å undersøke effekten på kompositttets elastiske stivhet som følge av en inklusjonsfase nummer to. Spesielt er den generelle to-fase Mori-Tanaka-modellen utvidete til tre faser. Nye modeller er også presentert, der disse er modifiserte og utvidede versjoner av modellene som er beskrevet i litteraturen. Modellresultatene er videre sammenliknet med eksperimentelle data for to nanopartikkel/epoksy-systemer.

Som en overordnet konklusjon, er det til en viss grad godt samsvar mellom modellresultatene for tre-fase-modellene og de eksperimentelle dataene. Ved å inkludere en inklusjonsfase nummer to, reduseres stivheten til kompositttet, forutsatt at stivheten til inklusjonsfasen er lavere enn matrisens. Derimot klarer ikke tre-fase-modellene å fange opp den veldig høye stivhetsøkningen som er observert eksperimentelt for lave volumfraksjoner; tre-fase-modellene ser generelt ut til å underestimere stivheten. Ett unntak er Paul-modellen, men denne modellen inkluderer ikke partiklenes geometri eksplisitt i uttrykkene, noe som gjør den mindre fleksibel for ulike kompositter. Videre studier bør derfor vurdere andre effekter enn de som er inkludert i modellene som er vist her. Spesielt er det relevant å etablere modeller som inkluderer en interfase, som kan modelleres som en region som omslutter partiklene, og som har andre elastiske egenskaper enn matrisen.

Contents

1 Introduction

This report describes mathematical modelling of the elastic stiffness of *nanocomposites*, which in this context is referred to as particles of nano-size included in a polymer matrix, i.e. particles with one dimension of nanometre size. The main motivation for this work is to establish a mathematical "model toolbox" for nanocomposites that can be used in future applications and for improving the understanding of this type of materials.

As described by Thorvaldsen [1], several factors have to be taken into consideration when modelling the elastic stiffness of nanocomposites; small particle weight/volume fractions, large particle interfacial area, particle aspect ratio, degree of dispersion and agglomeration, interphase effects, length and orientation distributions, load transfer and waviness (for fibre-like particles). In particular, obtaining nanocomposites with perfect dispersion of the particles, or even a high degree of dispersion, has been reported to be very challenging, due to, among other factors, the high viscosity of the nanomodified matrix when adding only a small weight per cent (wt%) of the filler material. Establishing tools for analyses of nanomodified matrix systems with a low degree of dispersion is therefore relevant, resulting in composites with more than one inclusion phase. In addition, it is relevant to investigate the effect of voids in the matrix, i.e. a composite where the second inclusion phase represents areas in the matrix with zero stiffness.

Models are described where one considers both free particles and agglomerates. One attempt is the three-phase rule of mixtures model for carbon nanotubes (CNTs) presented by Thorvaldsen *et al.* [2]. This model considers both free CNTs, agglomerates of CNTs, as well as the neat matrix. This model, however, contains several model parameters from different sub models. First of all, it is challenging to get all the required parameter values. Second, the combination of sub models makes it difficult to apply the correct volume fractions of each phase in the step-wise calculation of the composite stiffness. Other three-phase models are also established for two-phase regions in a matrix, i.e. particles embedded in other particles, which again are embedded in a matrix [3].

To extend the existing "model toolbox" for calculating the elastic stiffness of nanocomposites [1;4-6], *three-phase models* based on the Mori-Tanaka method and other approaches are described, implemented and compared in this report. Moreover, the model calculations are compared with experimental data where available. The same assumptions as made in [1] for the composites are also applied in the current study, except for the extension to three-phase nanocomposites.

2 Mathematical model

In this section, different models for three-phase nanocomposites are described. This includes a general Mori-Tanaka model for three (or more) phases, as well as specialized expressions for some three-phase composites.

2.1 A general three-phase Mori-Tanaka model

A general multi-phase Mori-Tanaka model for composites has been described in [1], including the theory of the Eshelby tensor. The Eshelby tensor for the different geometries is explicitly given in the referred report.

As a short summary, the general expression for the elastic stiffness of composites with *aligned spheroidal inclusions* is given as

$$C_{C,alligned} = V_0 C_0 A_0 + \sum_{r=1}^{N-1} V_r C_r A_r = \left(V_0 C_0 + \sum_{r=1}^{N-1} V_r C_r A_r^{dil} \right) \left(V_0 I + \sum_{r=1}^{N-1} V_r A_r^{\mathrm{dil}} \right)^{-1} \tag{2.1}$$

For composites with *randomly oriented inclusions* the elastic stiffness is written,

$$C_{C,random} = \left(V_0 C_0 + \sum_{r=1}^{N-1} V_r \{ C_r A_r^{dil} \} \right) \left(V_0 I + \sum_{r=1}^{N-1} V_r \{ A_r^{\mathrm{dil}} \} \right)^{-1} \tag{2.2}$$

In the above expressions, V_0 is the volume fraction of the matrix, whereas V_r is the volume fraction of the rth inclusion phase. Moreover, C_0 is the stiffness of the matrix, and C_r is the stiffness of the rth inclusion phase. Furthermore, A_0, A_r and A_r^{dil} are functions of the stiffness of the constituent materials of the composite, as well as the Eshelby tensor S_r (not explicitly shown in the above expressions). The curly brackets in (2.2) indicate that the quantities are orientationally averaged. For three-phase cases, $N = 3$ in the above expressions.

2.2 Specialized expression for a three-phase composite

Weng [7] has presented a model for a three-phase composite, which is based on the Mori-Tanaka method. The composite bulk and shear moduli may in this model be written as

$$\begin{aligned} \frac{\kappa_{comp}}{\kappa_0} &= 1 + \frac{a}{1 - \alpha_0 a} \\ \frac{\mu_{comp}}{\mu_0} &= 1 + \frac{b}{1 - \beta_0 b} \end{aligned} \tag{2.3}$$

where

$$\begin{aligned} a &= \sum_r \frac{c_r (\kappa_r - \kappa_0)}{\alpha_0 (\kappa_r - \kappa_0) - \kappa_0} \\ b &= \sum_r \frac{c_r (\mu_r - \mu_0)}{\beta_0 (\mu_r - \mu_0) - \mu_0} \end{aligned} \tag{2.4}$$

These general expressions for calculating the elastic properties of a three-phase composite may then be written as follows:

$$\frac{\kappa_{comp}}{\kappa_0} = 1 + \frac{\alpha_0(\kappa_1-\kappa_0)(\kappa_2-\kappa_0) + c_1\kappa_0(\kappa_1-\kappa_0) + c_2\kappa_0(\kappa_2-\kappa_0)}{\kappa_0^2 + c_1\alpha_0\kappa_0(\kappa_2-\kappa_0) + c_2\alpha_0\kappa_0(\kappa_1-\kappa_0)}$$
$$\frac{\mu_{comp}}{\mu_0} = 1 + \frac{\beta_0(\mu_1-\mu_0)(\mu_2-\mu_0) + c_1\mu_0(\mu_1-\mu_0) + c_2\mu_0(\mu_2-\mu_0)}{\mu_0^2 + c_1\beta_0\mu_0(\mu_2-\mu_0) + c_2\beta_0\mu_0(\mu_1-\mu_0)} \quad (2.5)$$

In the above expressions, κ_i is the isotropic bulk modulus, and μ_i is the shear modulus of the matrix phase ($i = 0$) and the inclusion phases ($i = 2,3$). Moreover, following the syntax of Weng, c_0, c_1 and c_2 are the volume fraction of the matrix and inclusion phases, respectively, with $c_0 + c_1 + c_2 = 1$. Finally,

$$\alpha_0 = \frac{3\kappa_0}{3\kappa_0 + 4\mu_0}$$
$$\beta_0 = \frac{6}{5}\frac{\kappa_0 + 2\mu_0}{3\kappa_0 + 4\mu_0} \quad (2.6)$$

The elastic modulus of the composite can then be expressed as,

$$\frac{E_{comp}}{E_m} = \frac{\kappa_{comp}\mu_{comp}(3\kappa_0 + \mu_0)}{3\kappa_{comp}\kappa_0 + \mu_{comp}\mu_0} \quad (2.7)$$

where the composite stiffness is normalized by the matrix Young's modulus E_m (or E_0).

In the example presented by Weng, the three phases are quartz sand fillers, the matrix, and voids within the matrix. The model should, however, not necessarily be restricted to the case of having quartz sand particles as one of the inclusion phases.

2.3 Analytical expression for three-phase composites including voids

Two different model approaches, which are *not* based on the Mori-Tanaka method, are presented for particulate composites with a porous matrix, i.e. composites containing voids in addition to nanoparticles.

2.3.1 Uniform displacement assumption

Cohen and Ishai [8;9] base their model on a cubic model, where a cubic inclusion is embedded in a cubic matrix. The boundaries are in this case subjected to a uniform displacement. The filler content is assumed to be in the range of 20 to 50 volume per cent, making the approximate approaches okay for practical use of the models. The model is, however, tested in the range from zero to about 50 volume per cent. It should also be emphasized that the filler content of nanoparticles (for which we want to apply the models) is typically less than 20 volume per cent.

First, assuming a voidless matrix, the elastic modulus of the particulate composite can be expressed as,

$$E_C = E_m \left[1 + \frac{V_f}{\frac{m}{m-1} - \sqrt[3]{V_f}} \right] \tag{2.8}$$

where E_m is the elastic modulus of the matrix, $m = E_f / E_m$, with E_f the Young's modulus of the filler, and $V_f = \upsilon_f / \upsilon_C$ the volumetric filler content, i.e. the volume fraction.

Second, assuming a porous matrix including voids, a modified version of the above expression can be established,

$$E_C = E_m (1 - V_v^{*\,2/3}) \left[1 + \frac{V_f}{\frac{m^*}{m^* - 1} - \sqrt[3]{V_f}} \right] \tag{2.9}$$

where the Young's modulus of the voidless matrix is now replaced by the matrix-void system, $E_v^* = E_m (1 - V_v^{*\,2/3})$, with V_v^* the void content, and $m^* = E_f / E_v^*$. It is assumed that the presence of the filler material does not affect the properties of the porous matrix.

2.3.2 Uniform stress assumption

Paul [8;10] suggested a similar model as Cohen and Ishai (see Section 2.3.1), but assumed that the boundary condition is that of uniform stress. The model is derived for a metal reinforced with another metal of higher elastic stiffness.

The expression for a particulate composite with a voidless matrix, can in this case be written as

$$E_C = E_m \left[\frac{1 + (m-1) V_f^{2/3}}{1 + (m-1)(V_f^{2/3} - V_f)} \right] \tag{2.10}$$

where the parameters are described in Section 2.3.1.

Based on Paul's derivation, the expression for the elastic modulus of a particulate composite with a porous matrix (i.e. matrix including voids) then reads

$$E_C = E_m \left[\frac{1 - V_v^{*\,2/3}}{1 - V_v^{*\,2/3} + V_v^*} \right] \left[\frac{1 + (m^* - 1) V_f^{2/3}}{1 + (m^* - 1)(V_f^{2/3} - V_f)} \right] \tag{2.11}$$

Here, the elastic constant for the porous matrix E_{cv} can be written as

$$E_{cv} = E_m \left[\frac{1 - V_v^{*\,2/3}}{1 - V_v^{*\,2/3} + V_v^*} \right] \tag{2.12}$$

2.4 Analytical expression for three-phase composites including agglomerates

Using the models presented by Cohen and Ishai [8;9] and Paul [10] as a starting point, *new* analytical expressions may be derived for three-phase composites with one phase being agglomerates of the filler material (with a reduced stiffness) instead of voids (with no stiffness). This will fit into the framework of model cases presented by both Cohen and Ishai and Paul, as well as the one by Weng [7], see Section 2.2. Since the expressions presented in Section 2.3 are established from different assumptions concerning the boundary conditions, two different models are also established here.

There is one main challenge with applying the current suggested new methods: the elastic parameters for the agglomerates. If assuming, for simplicity, isotropic material properties of the agglomerates, the number of material constants is reduced to two, i.e. the Young's modulus and the Poisson's ratio.

2.4.1 Uniform displacement assumption

Considering the expression in (2.8), but now assuming a two-phase agglomerate/matrix composite, we can define

$$\hat{m} = \frac{E_a}{E_m} \tag{2.13}$$

where E_a is the elastic stiffness of the agglomerates. Moreover, with $\upsilon_m + \upsilon_a = \upsilon_C$, where υ_a is the volume of agglomerates, we get that the agglomerate content can be written as,

$$V_a = \frac{\upsilon_a}{\upsilon_a + \upsilon_m} = \frac{\upsilon_a}{\upsilon_C} \tag{2.14}$$

The elastic modulus of the agglomerate/matrix composite E_{ca} may then be expressed as

$$E_{ca} = E_m \left[1 + \frac{V_a}{\frac{\hat{m}}{\hat{m}-1} - \sqrt[3]{V_a}} \right] \tag{2.15}$$

From this, the elastic stiffness of a three-phase composite, with filler and a porous matrix (containing agglomerates), may be written,

$$E_C = E_m \left[1 + \frac{V_a}{\frac{\hat{m}}{\hat{m}-1} - \sqrt[3]{V_a}} \right] \left[1 + \frac{V_f}{\frac{m^*}{m^*-1} - \sqrt[3]{V_f}} \right] \tag{2.16}$$

where now $m^* = E_f / E_{ca}$. The remaining parameters are given in Section 2.3.1.

In the following, this model is referred to as the Cohen-Ishai-Thorvaldsen model to distinguish it from the original Cohen-Ishai model.

2.4.2 Uniform stress assumption

Consider the expression in (2.10), and assuming a two-phase agglomerate/matrix composite, with $\hat{m}$ given in (2.13), and following the same approach as in Section 2.4.1, the elastic modulus of the agglomerates/matrix composite can be expressed as,

$$E_{ca} = E_m \left[\frac{1 + (\hat{m}-1)V_a^{2/3}}{1 + (\hat{m}-1)(V_a^{2/3} - V_a)} \right] \tag{2.17}$$

The three-phase filler/agglomerate/matrix composite may now be written as

$$E_C = E_m \left[\frac{1 + (\hat{m}-1)V_a^{2/3}}{1 + (\hat{m}-1)(V_a^{2/3} - V_a)} \right] \left[\frac{1 + (m^*-1)V_f^{2/3}}{1 + (m^*-1)(V_f^{2/3} - V_f)} \right] \tag{2.18}$$

In the following, this model is referred to as the Paul-Thorvaldsen model, to distinguish it from the original Paul model.

3 Composite material systems

Two different composite material systems are included in the current study. For both systems, experimental data are available from the literature.

3.1 Material data

The material data applied for the nanoalumina/epoxy composite are given in Table 3.1 [4]. Both the matrix and the alumina particles are considered having isotropic material properties.

Table 3.1 Material data for nanoalumina/epoxy composites, with elastic properties from [4].

Material parameter	Unit	Value
Matrix:		
Young's modulus	GPa	3.12
Poission's ratio		0.35
Inclusion:		
Young's modulus	GPa	386
Poission's ratio		0.22

The material data applied for the nanosilica/epoxy composite are given in Table 3.2 [11]. Both the matrix and the silica particles are considered having isotropic material properties.

Table 3.2 Material properties for nanosilica/epoxy composites, with elastic properties from [11].

Material parameter	Unit	Value
Matrix:		
Young's modulus	GPa	2.96
Poisson's ratio		0.35
Silica inclusion:		
Young's modulus	GPa	70
Poisson's ratio		0.20

3.2 Experimental data

For the nanoalumina/epoxy composite, experimental data are available in [4]. The measured composite elastic stiffness values are given in

Table 3.3 and Table 3.4 for spherical and fibre-like inclusions, respectively. Different techniques are applied for obtaining a good dispersion, i.e. bath sonication and horn sonication. In addition, for the spherical particles a surface treatment was applied prior to dispersion. The surface treatment is believed to improve the load transfer from the particle to the matrix. More details are found in [4].

Table 3.3 Experimental results for the elastic properties of alumina/epoxy nanocomposites with spherical inclusions. The data are taken from [4].

Material type	Sonication	wt%	Nominal V_f	Tensile modulus, E (MPa)
Epoxy	N/A	N/A	0.0	3120 ± 110
NT-50nm	Bath	1.0	0.00350	3150 ± 100
NT-50nm	Bath	4.0	0.01385	3220 ± 130
NT-50nm	Horn	1.0	0.00345	3400 ± 190
NT-50nm	Horn	2.9	0.01025	3240 ± 70
GPS-50nm	Bath	3.0	0.01060	3290 ± 130
GPS-50nm	Horn	1.0	0.00345	3130 ± 60

(NT = Non-treated; GPS = silane treated)

Table 3.4 Experimental results for the elastic properties of alumina/epoxy nanocomposites with fibre-like inclusions. The data are taken from [4].

Material type	Sonication	wt%	Nominal V_f	Tensile modulus, E (MPa)
Epoxy	N/A	N/A	0.0	3120 ± 110
NT-wiskers	Bath	0.1	0.00035	3310 ± 140
NT-wiskers	Bath	1.0	0.00350	3360 ± 110
NT-wiskers	Bath	3.0	0.01060	3450 ± 170
NT-wiskers	Bath	5.0	0.01730	3540 ± 130
NT-wiskers	Horn	0.1	0.00035	3210 ± 190
NT-wiskers	Horn	1.0	0.00345	3390 ± 120
NT-wiskers	Horn	2.9	0.01025	3360 ± 140

(NT=Non-treated; GPS = silane treated)

For the nanosilica/epoxy composite, experimental data are available in [11]. The measured composite elastic stiffness values are given in Table 3.5.

Table 3.5 Experimental results for the elastic properties of silica/epoxy composites with spherical inclusions. The data are taken from [11].

Material type	wt%	Nominal V_f	Tensile modulus, E (MPa)
Epoxy	N/A	0.0	2960 ± 200
Nanosilica-epoxy	4.1	0.025	3200 ± 150
Nanosilica-epoxy	7.8	0.049	3420 ± 180
Nanosilica-epoxy	11.1	0.071	3570 ± 130
Nanosilica-epoxy	14.8	0.096	3600 ± 50
Nanosilica-epoxy	20.2	0.134	3850 ± 240

4 Numerical results

In this section, the calculated composite elastic stiffness as a function of volume fraction of the different constituents is plotted for the models described in Section 2. The composite material systems given in Section 3.1 are applied. For the two included systems, experimental data are also available, as given in Section 3.2.

4.1 Two-phase voids/epoxy models

For validation of the model implementation, the two-phase voids/epoxy composite models by Cohen and Ishai and Paul, described in Section 2.3, are plotted together with the general two-phase Mori-Tanaka model, described in Section 2.1. The stiffness values are shown in Figure 4.1, where the two-phase Cohen-Ishai model is given by the black curve and the Paul model is given by the blue curve. These two curves agree with the results and the plot shown in the paper by Cohen and Ishai [8]. The general two-phase Mori-Tanaka model, based on the assumption of spherical shaped voids, gives similar results (red curve). The Mori-Tanaka model, however, estimates a lower composite stiffness as a function of void fraction, compared to the Paul model, but is closer to the composite stiffness calculated by the Cohen-Ishai model.

As a general conclusion from this case, the elastic stiffness of a composite is reduced as a function of void fraction. This is as expected.

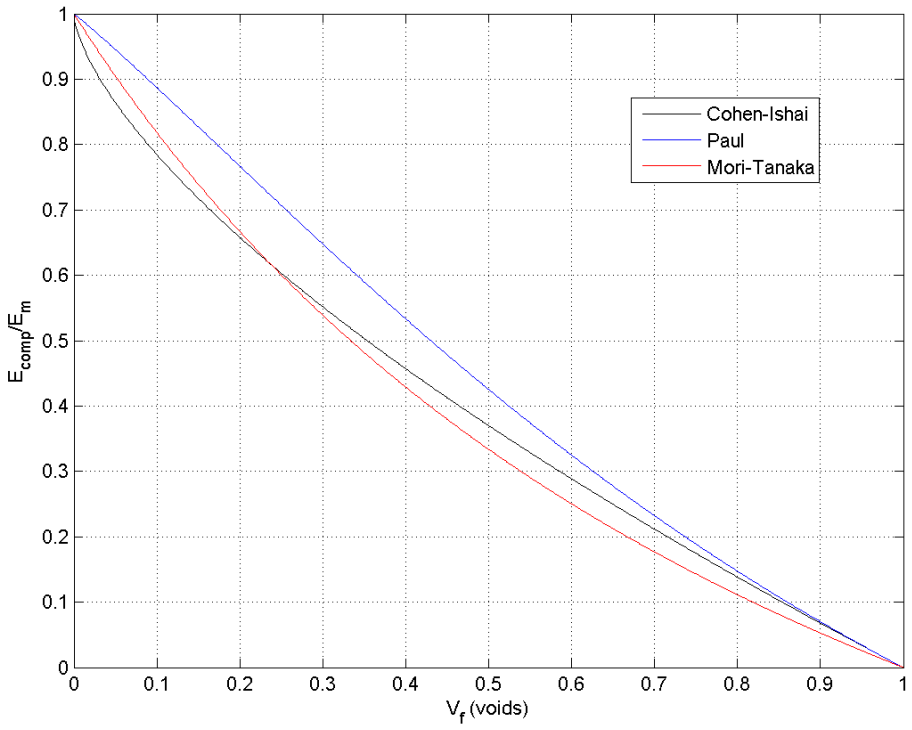

Figure 4.1 Composite elastic stiffness of epoxy with voids. Three different two-phase models are plotted.

4.2 Three-phase models with voids

4.2.1 Alumina/epoxy composite

Figure 4.2 shows the calculations of the elastic stiffness for a composite with nanoalumina particles and voids included in the epoxy matrix (Table 3.1), as well as the available experimental data for spherical particles (Table 3.4). The Cohen-Ishai, Paul and the three-phase Mori-Tanaka models are included in the plot.

For all three models, the volume fraction of the alumina particles (V_f) is varied. In each case, the void volume fraction (V_a) is either zero, i.e. a void-free particulate composite, or set to 0.005.

The void-free case is shown by the solid line, whereas the case of a constant void volume fraction is shown by a dotted line. For the Mori-Tanaka model, spherical inclusions is applied for both the particles and the voids.

As can be seen from the plot, the Paul model predicts a much higher composite stiffness compared to the Mori-Tanaka model and the Cohen-Ishai model. Including a small volume fraction of voids in the matrix, the elastic stiffness is reduced. Comparing the model results to the experimental data, we find that the Paul model is able to predict the large increase in composite stiffness for low volume fractions of alumina particles, but overestimates the stiffness for higher volume fractions. The Cohen-Ishai model generally underestimates the composite stiffness for all concentrations. The Mori-Tanaka calculations are in agreement with some of the experimental data points, but generally underestimates the stiffness. As commented by Cohen and Ishai [8], their approach and the Paul approach may be seen as upper and lower limits for the real stiffness. More test data are required before concluding on the agreement between the model calculations and the experimental results.

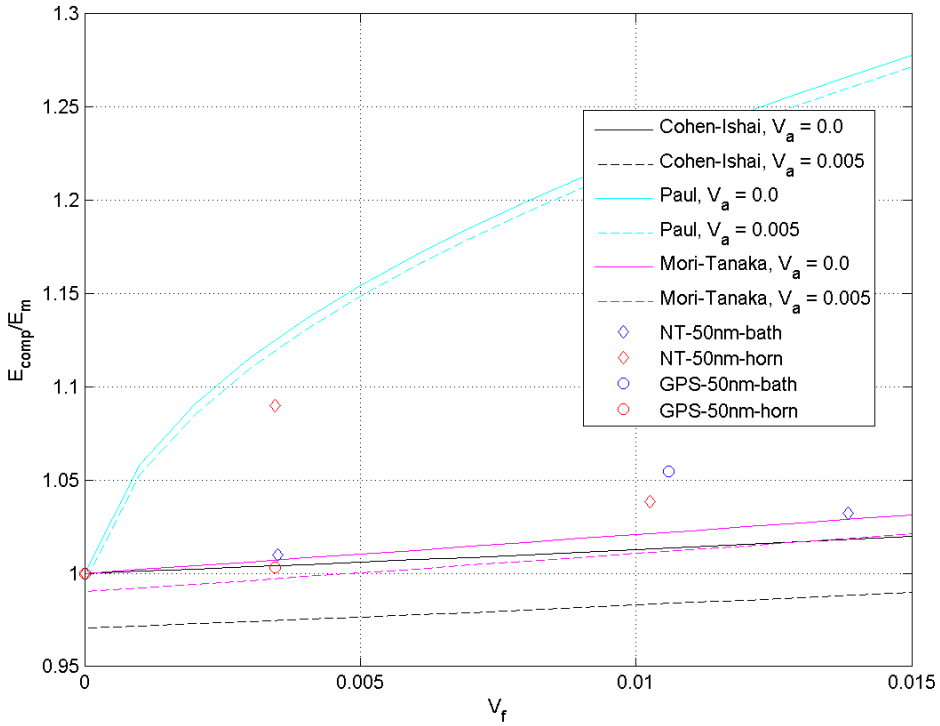

Figure 4.2 Elastic stiffness of a composite with particles, without voids ($V_a = 0.0$) or with voids ($V_a = 0.005$). The Cohen-Ishai, Paul and the Mori-Tanaka models are plotted. For the general Mori-Tanaka model, spherical inclusions are applied for both inclusion phases. The experimental data are taken from Johnsen et al. [4].

4.2.2 Silica/epoxy composites

Figure 4.3 shows the calculations of the elastic stiffness for a composite with nanosilica particles and voids included in the epoxy matrix (Table 3.2), as well as the available experimental data (Table 3.5). The Cohen-Ishai, Paul and the three-phase Mori-Tanaka models are included in the plot.

For all three models, the volume fraction of the silica particles (V_f) is varied. In each case, the void volume fraction (V_a) is either zero, i.e. a void-free particulate composite, or set to 0.005. The void-free case is shown by the solid line, whereas the case of a constant void volume fraction is shown by a dotted line. For the Mori-Tanaka model, spherical inclusions is applied for both the particles and the voids.

As can be seen from this plot, the Paul model predicts a much higher composite stiffness than the Mori-Tanaka model and the Cohen-Ishai model. When including a small volume fraction of voids in the matrix, the composite elastic stiffness is reduced.

Comparing the model results to the experimental data, we find that the Paul model overestimates the stiffness for all concentrations. The Cohen-Ishai model generally underestimates the composite stiffness for all concentrations. The Mori-Tanaka calculations are in agreement with some of the experimental data points, but generally seem to underestimate the stiffness for low

volume fractions of silica particles. As commented by Cohen and Ishai [8], and commented for the previous composite system, their approach and the Paul approach may be seen as upper and lower limits for the real stiffness.

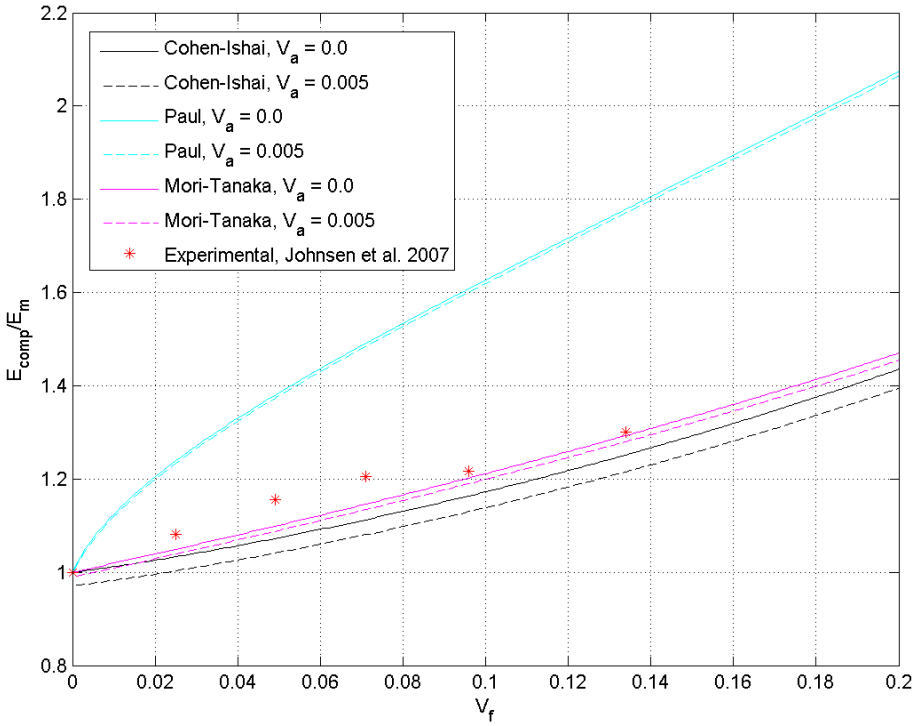

Figure 4.3 Elastic stiffness of a composite with particles, without voids ($V_a = 0.0$) or with voids ($V_a = 0.005$). The Cohen-Ishai, Paul and the Mori-Tanaka models are plotted. For the general Mori-Tanaka model, spherical inclusions are applied for both inclusion phases. The experimental data are taken from Johnsen et al. [11].

4.3 Three-phase models with agglomerates

4.3.1 Weng three-phase model

Figure 4.4 displays the Weng three-phase model, see Section 2.2. In this case, the inclusion phases are spherical in shape. For all cases, the agglomerate volume fraction is 0.01. The alumina/epoxy material system data is applied in the plot. The calculated stiffness is compared to and found to agree with the model results using the general three-phase Mori-Tanaka method with spherical inclusions, see Section 2.1.

As displayed in the figure, the elastic stiffness of the agglomerates is varied to see the effect on the composite elastic stiffness from such inclusions. The green curve displays the case where the second inclusion phase has the same stiffness properties as the matrix. The stiffness of the composite is then equal to the stiffness obtained from a two-phase alumina/epoxy model, as shown in [1]. The blue curve displays the case where the agglomerates have zero stiffness, i.e. voids. The stiffness is reduced for all particle volume fractions. This is as expected. The red curve shows the case where the stiffness of the agglomerates is about one third of the matrix stiffness.

The stiffness of the composite is reduced compared to the two-phase composite, but is higher than for composites with voids. Finally, the magenta curve shows the case where the stiffness of the agglomerates is about three times the stiffness of the matrix. The stiffness of the composites is higher than the two-phase composite. This latter case is, however, not believed to be physically meaningful.

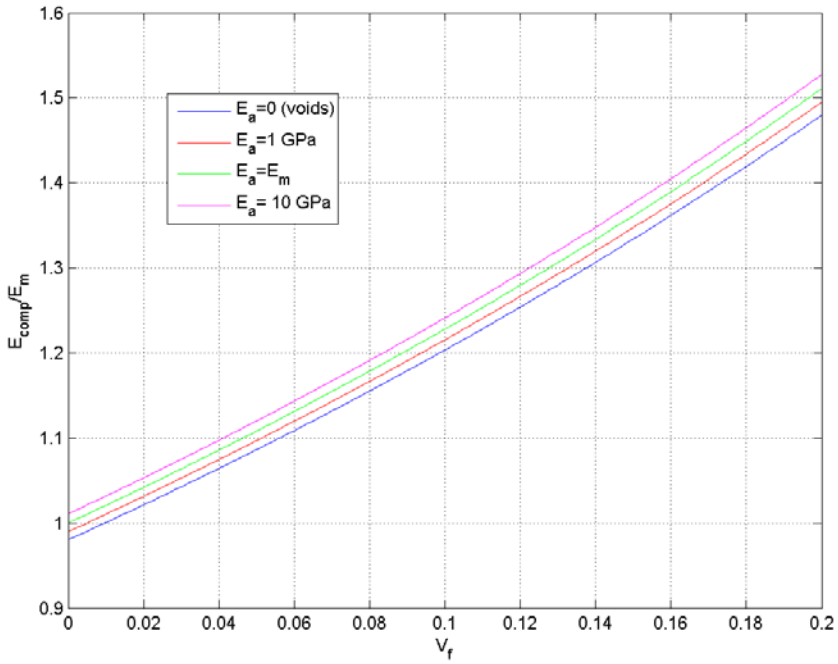

Figure 4.4 The Weng and the Mori-Tanaka three-phase models for particulate composites with agglomerates. Both the particles and the agglomerates have a spherical shape. The volume fraction of agglomerates is 0.01.

4.3.2 The three-phase Mori-Tanaka model

4.3.2.1 Nanoalumina/epoxy composite

The three-phase Mori-Tanaka model results are compared to the experimental data for the alumina/epoxy composite with spherical particles. Three different shapes are included in the modelling: 1) spheres (aspect ratio $\alpha = 1$) , 2) slightly prolate shape (aspect ratio $\alpha = 3$), and 3) slightly oblate shape (aspect ratio $\alpha = 0.5$). For each shape, two different cases are run: a) zero agglomerates, and b) an agglomerate volume fraction of 0.005. The agglomerate elastic stiffness is set to 1 GPa, which is about one third of the matrix stiffness.

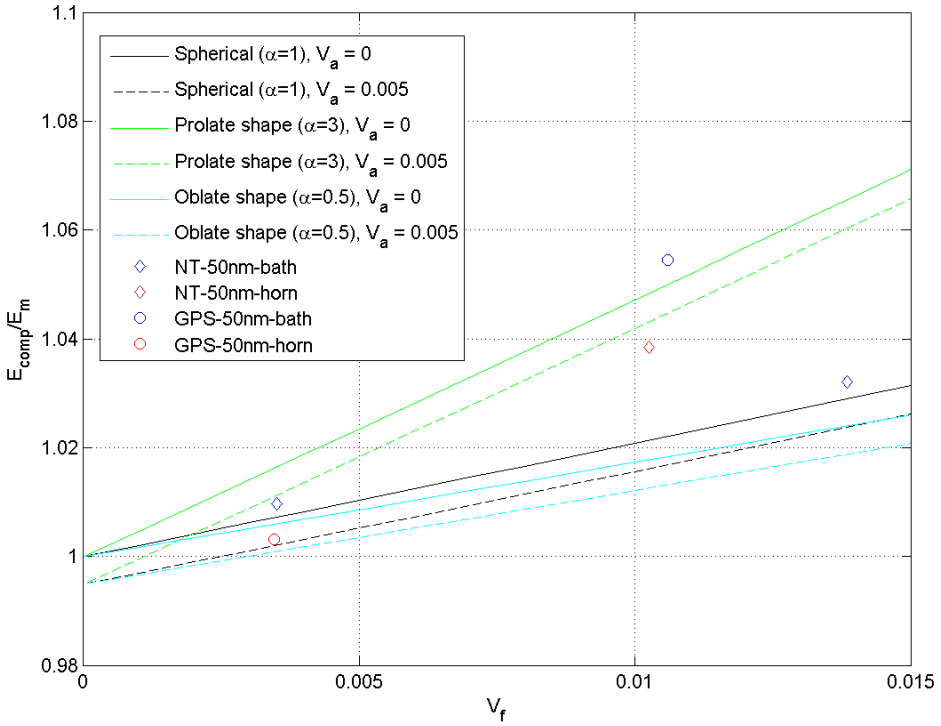

Figure 4.5 Alumina spheres/epoxy/agglomerates composite. Three different spheroidal shapes are included. The numerical calculations are plotted together with experimental results [4].

Figure 4.5 shows the composite elastic stiffness as a function of free particles. As can be observed, agglomerates reduce the composite elastic stiffness for all volume fractions. The test data for the specimens with untreated particles using bath sonication agrees well with the calculated stiffness for spherical particles when no agglomerates are present. Moreover, the GPS treated particles using bath sonication agree well with the calculated stiffness for prolate shaped particles when no agglomerates are present. The test data for the test specimens with untreated particles using horn sonication are more in accordance with the calculated stiffness for prolate shaped particles when agglomerates are present. Finally, the test data for the specimens with the GPS treated particles using horn sonication agree with the calculated stiffness for spherical particles when agglomerates are present.

Note that in the above plot, the model calculations assume a particle volume fraction as the sum of free particles (V_f) and the agglomerated particles, and where the amount of free particles is indicated on the horizontal axis. The experimental data points, however, are based on the measured composite elastic stiffness for the test specimen, where different volume fractions of particles (V_f) is included in the matrix. No detailed information is available for the degree of dispersion, i.e. the amount free particles and the amount of particles in agglomerates. In case the (physical) test specimens contain agglomerates, the volume fraction of free particles is lower (than plotted).

4.3.2.2 Nanosilica/epoxy composite

The calculated stiffness using the three-phase Mori-Tanaka model is compared to the experimental data for the silica/epoxy composite. Three different shapes are included in the modelling: 1) spheres (aspect ratio $\alpha = 1$) , 2) slightly prolate shape (aspect ratio $\alpha = 3$), and 3) slightly oblate shape (aspect ratio $\alpha = 0.5$). For each shape, two different cases are run: a) zero agglomerates, and b) an agglomerate volume fraction of 0.005. The agglomerate elastic stiffness is set to 1 GPa, which is about one third of the matrix stiffness.

Figure 4.6 shows the composite elastic stiffness as a function of free particles. As can be observed, the inclusion of agglomerates slightly reduces the composite elastic stiffness for all volume fractions of free silica particles. Composites with spherical shaped particles seem to underestimate the composite stiffness for low volume fractions, but agree very well for high volume fractions. Composites with slightly prolate shaped particles seem to better predict the composite stiffness for low volume fractions. For higher volume fractions, the composites with prolate shaped particles overestimate the composite stiffness. The composites with oblate particles underestimate the composite stiffness for all volume fractions.

As commented for the nanoalumina/epoxy system in Section 4.3.2.1, the actual volume fraction of free particles in the physical test specimens may be lower than indicated in the plot, in case part of the particles are contained in agglomerates. Johnsen *et al.*[11], however, report a very high degree of exfoliation, which means that the actual volume fractions are very close to the fractions applied in the plot.

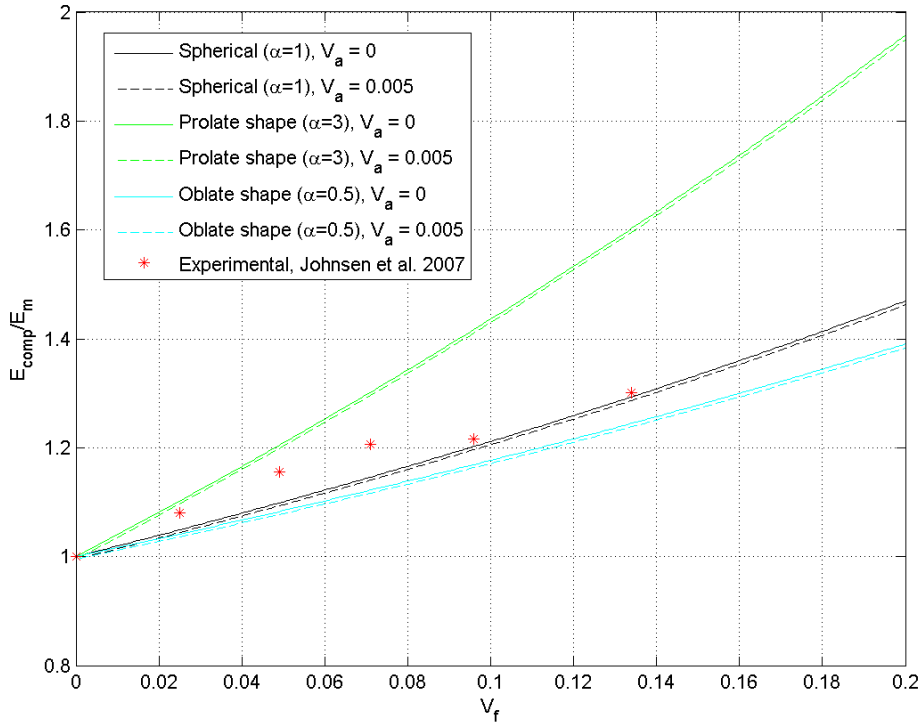

Figure 4.6 Silica spheres/epoxy/agglomerate composite. Three different spheroidal shapes are included. The numerical calculations are plotted together with experimental results [11].

4.3.3 Cohen-Ishai-Thorvaldsen and Paul-Thorvaldsen models

The modified three-phase Cohen-Ishai and Paul models, where a second inclusion phase is included, with a stiffness different from the free particles, but higher than zero (i.e. voids), is analysed in this section. The model results are compared with the three-phase Mori-Tanaka model for spherical particle/epoxy composites.

For all three models, the volume fraction of the alumina particles (V_f) is varied. In each case, the agglomerate volume fraction V_a is either zero, i.e. a particulate composite with perfect dispersion, or set to 0.005. The agglomerate-free case is shown by the solid line, whereas the case of a constant agglomerate volume fraction is shown by the dotted line. For the three-phase Mori-Tanaka model, spherical inclusions are applied for both the particles and the agglomerates. The stiffness of the agglomerates is set to 1 GPa.

4.3.3.1 Nanoalumina/epoxy composite

Figure 4.7 displays the calculated composite stiffness for the nanoalumina/epoxy composite, together with the experimental results for the nanoalumina/epoxy composite.

As can be seen from the plot, the Paul-Thorvaldsen model predicts a much higher composite stiffness compared to the Mori-Tanaka model and the Cohen-Ishai-Thorvaldsen models. Including a small volume fraction of agglomerates in the matrix, results in a reduction in the composite elastic stiffness. The composite stiffness is, however, higher in this case, compared to including voids. This is as expected.

Comparing the model results to the experimental data, we find that the Paul-Thorvaldsen model is able to predict the large increase in composite stiffness for low volume fractions of alumina particles, but seems to overestimate the stiffness for higher volume fractions. The Cohen-Ishai-Thorvaldsen model generally underestimates the composite stiffness for all concentrations. The Mori-Tanaka calculations are in agreement with some of the data points, but generally also seem to underestimate the composite stiffness.

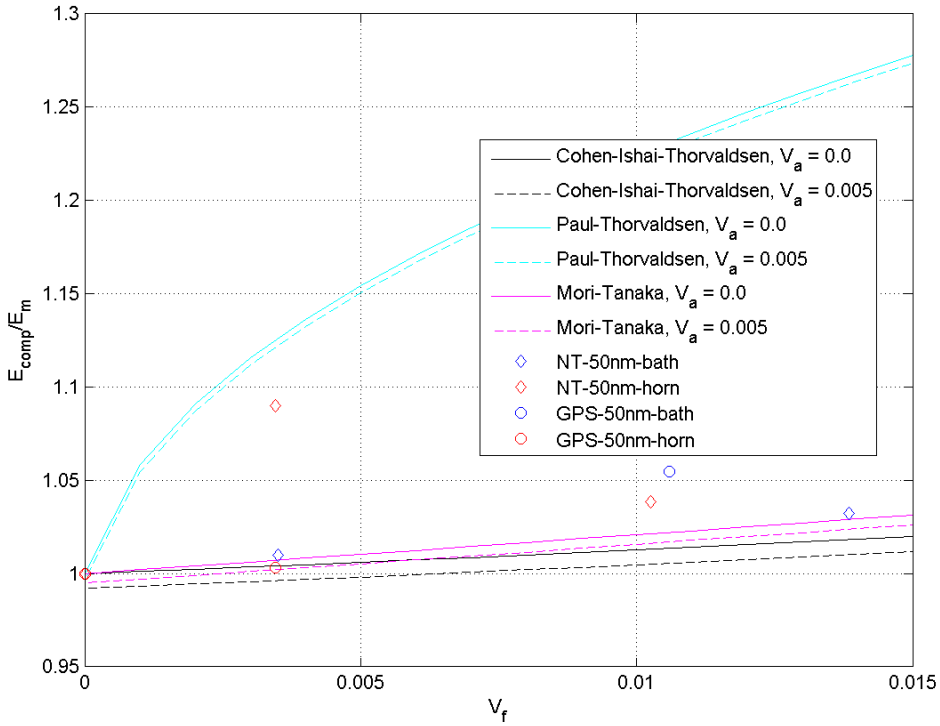

Figure 4.7 Three-phase model with agglomerates. New models based on the Cohen-Ishai-Thorvaldsen and Paul-Thorvaldsen models. The numerical calculations are plotted together with experimental results [4].

4.3.3.2 Nanosilica/epoxy composite

Figure 4.8 shows the calculated elastic stiffness for the nanosilica/epoxy composite particles, together with the experimental results for the nanosilica/epoxy composite.

As can be seen from the plot, the Paul-Thorvaldsen model predicts a much higher composite stiffness compared to the Mori-Tanaka model and the Cohen-Ishai-Thorvaldsen model. Including a small volume fraction of agglomerates in the matrix, the composite elastic stiffness is slightly reduced.

Comparing the model results to the experimental data, we find that the Paul-Thorvaldsen model generally overestimates the stiffness. The Cohen-Ishai-Thorvaldsen model generally underestimates the composite stiffness for all concentrations. The Mori-Tanaka calculations are in agreement with the experimental data for high volume fractions, but underestimates the stiffness for low volume fractions of silica particles.

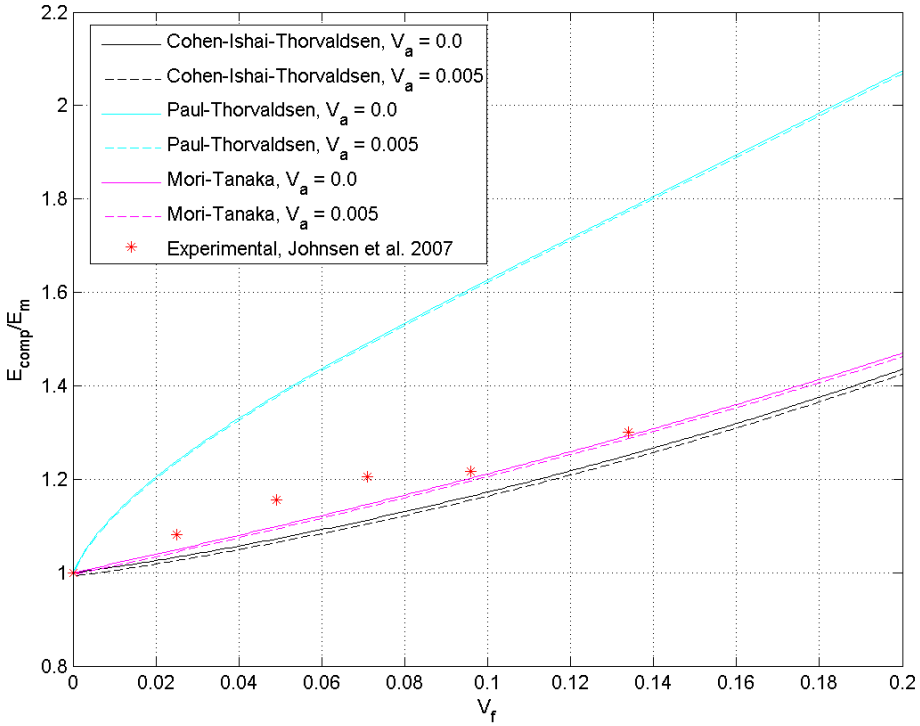

Figure 4.8 Three-phase model with agglomerates. New models based on the Cohen-Ishai-Thorvaldsen and Paul-Thorvaldsen models. The numerical calculations are plotted together with experimental results [11].

4.4 Randomly oriented fibre-like inclusions and spherical agglomerate inclusions

As the final test case, the three-phase Mori-Tanaka model is applied for calculating the elastic stiffness of a nanocomposite with randomly oriented fibre-like particles in a polymer system, where a second inclusion phase is present.

Figure 4.9 displays the calculated elastic stiffness for the nanoalumina/epoxy composite with randomly oriented whiskers. A second inclusion phase, being either voids with no stiffness, or agglomerates with a higher stiffness compared to the neat epoxy, is included.

Our reference in this case is the composite without agglomerates (black curve). By including a second inclusion phase, the composite stiffness is changed. If including voids (cyan curve), the matrix stiffness is reduces. If including a second (spherical) inclusion phase with higher stiffness (compared to the neat polymer), in this case 10 GPa, improves the elastic stiffness of the composite (magenta curve). Finally, the aspect ratio of the first inclusion phase (the alumina whiskers in this case) will affect the composite stiffness (green curve).

The aspect ratio and the elastic stiffness of the agglomerates in the model calculations are chosen to make a best fit with the available experimental data, without considering the physical validity or relevance. As can be observed, the best fit for low volume fractions is obtained by increasing the elastic stiffness of the agglomerates to a very high value. By also reducing the aspect ratio of

the particles, a good correspondence is also obtained for high volume fractions. A very high stiffness for the agglomerates is, however, considered as unphysical. Hence, the thee-phase Mori-Tanaka model is not able to predict the stiffness increase for low volume fractions very well. Other effects than a second phase in the form of agglomerates is required for explaining this.

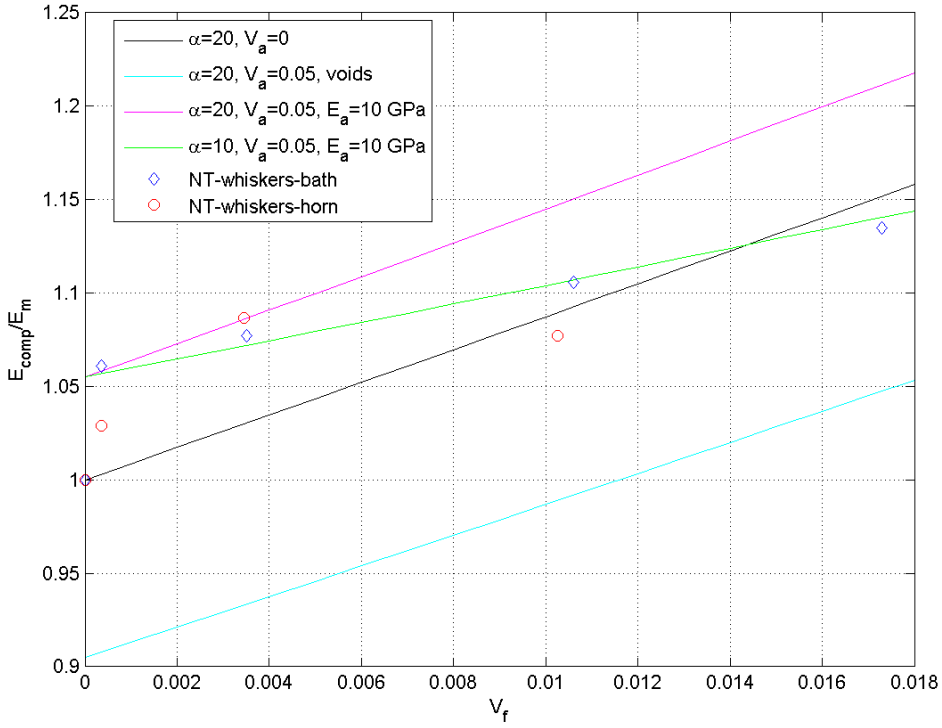

Figure 4.9 Composite elastic stiffness for randomly oriented whisker in a epoxy matrix using the three-phase Mori-Tanaka model. The experimental data are taken from Johnsen et al. [4].

5 Summary

In this report, models are presented for calculating the elastic stiffness of nanocomposites, with main focus on three-phase models, where a second inclusion phase, in addition to the nanoparticles, are contained in the polymer matrix. The general Mori-Tanaka model from [1] has been extended to three phases. A model by Weng for three-phase composites, also based on the Mori-Tanaka method, is also described. In addition, a set of two-phase and three-phase models for nanocomposites *not* based on the Mori-Tanaka method, has been described. These are the Cohen-Ishai and the Paul models. The latter models have been extended to also include a second inclusion phase with non-zero stiffness, i. e. agglomerates. For the included models, the Weng model is restricted to spherical particles, whereas the Cohen-Ishai model and the Paul model do not explicitly include the particle geometry. Only the general three-phase Mori-Tanaka model is applicable to different spheroidal inclusions, including spheres and oblate and prolate shaped inclusions.

Considering the model results, the three-phase Mori-Tanaka model calculations have been found to agree with the stiffness estimates obtained from using the Weng model. Moreover, the Paul model estimates a very high elastic stiffness, especially for low volume fractions. The Cohen-Ishai model estimates a much lower elastic stiffness for all volume fractions. The general three-phase Mori-Tanaka model estimates a stiffness that is slightly higher than the stiffness obtained from the Cohen-Ishai model. Including a second inclusion phase of either voids or agglomerates with a lower stiffness than the neat polymer, reduces the elastic stiffness for all volume fractions.

Comparing the calculated results with the experimental data for two different nanocomposites with spherical particles, the Paul model generally overestimates the elastic stiffness, whereas the Cohen-Ishai model underestimates the stiffness. The Mori-Tanaka model agrees well with the experimental data for high volume fractions, but underestimates the elastic stiffness for low volume fractions. The three-phase Mori-Tanaka model is also compared with experimental results for nanocomposites with non-spherical particles. Both the particle aspect ratio and the stiffness properties of the second inclusion phase (being voids or agglomerates) will influence on the composite elastic stiffness.

As a general conclusion, the three-phase Mori-Tanaka model is considered the best and most applicable model for different composites – even though the model is not able to predict the very high stiffness increase for low volume fractions. Follow-up studies should consider other factors than a second inclusion phase of voids or agglomerates, to better estimate the nanocomposite stiffness. One relevant factor is studying the effect on the composite stiffness due to interphase effects, which can be described by a region surrounding the nanoparticles with different elastic properties compared to the neat matrix.

Acknowledgements

The author would like to thank Bernt Brønmo Johnsen and Tyler P. Jones for reading the final version of this document and giving valuable comments and improvements to the text.

Appendix A Model summary

Table A.1 provides a summary of the implemented models described and presented in the report. Note that two of the models are two-phase models, which are included for validation of the code and the three-phase models.

The Matlab codes for all models are given in Appendix B.

Table A.1 Models for the two-phase and three-phase nanocomposites.

File name	References	Inclusion #1	Inclusion #2
three_phase_1.m	[1;12-14]	Spherical, fibre, or disc Aligned	Spherical, oblate, or prolate Aligned
three_phase_2.m	[1;12-14]	Spherical, fibre, or disc Random	Spherical, oblate, or prolate Aligned
weng_1.m	[7]	Particle	Agglomerate or void
cohen_ishai_1.m	[8;9]	Particle or void	N/a
cohen_ishai_2.m	[8;9]	Particle	Void
paul_1.m	[10]	Particle or void	N/a
paul_2.m	[10]	Particle	Void
three_phase_3.m	[8;9] (*)	Particle	Particle or agglomerate
three_phase_4.m	[10] (**)	Particle	Particle or agglomerate

(*) New model. Based on the Cohen-Ishai model.

(**) New model. Based on the Paul model.

Appendix B Matlab code

B.1 Cohen-Ishai two-phase model

```
% Cohen and Ishai two-phase model
% This case: One type of isotropic inclusions
% Reference: Cohen and Ishai, 1967
%
% Author: Tom Thorvaldsen, FFI, March 2014

% Stiffness - matrix
E_m = 3.12
nu_m = 0.35;

% Stiffness - inclusion
E_f = 0.0 % voids
nu_f = 0.35

m = E_f/E_m;
V_f = 0.0:0.001:1.0

for i = 1:length(V_f)
  E_comp = E_m*(1+(V_f(i)/((m/(m-1))-nthroot(V_f(i),3))))
  E_11(i) = E_comp/E_m;
end

plot(V_f,E_11,'k')
xlabel ('V_f')
ylabel('E_{comp}/E_0')
```

B.2 Paul two-phase model

```
% Paul two-phase model
% This case: One type of isotropic inclusions
% References: Paul, 1960
%
% Author: Tom Thorvaldsen, FFI, March 2014

% Stiffness - matrix
E_m = 3.12
nu_m = 0.35

% Stiffness - inclusion
E_f = 0.0 % voids
```

```
nu_f = 0.35

m = E_f/E_m;

V_f = 0.0:0.001:1.0

for i = 1:length(V_f)
  E_comp = E_m*((1+(m-1)*power(V_f(i),2/3))/(1+(m-1)*(power(V_f(i),2/3)-
V_f(i))))
  E_11(i) = E_comp/E_m;
end

plot(V_f,E_11,'b')
xlabel ('V_f (voids)')
ylabel('E_{comp}/E_0')
```

B.3 General three-phase Mori-Tanaka model for aligned inclusions

```
% General Mori-Tanaka three-phase model
% This case: Two types of isotropic inclusions
% Three geometries:
% 1) aligned spherical inclusions
% 2) aligned fibre-like inclusions with aspect ratio
% 3) aligned disc-shaped inclusion with apsect ratio
%
% Author: Tom Thorvaldsen, FFI, March 2014

% MATERIAL PARAMETERS
% Elastic properties - matrix
E_0 = 3.12
nu_0 = 0.35

C = zeros (6,6);
const = (E_0*(1-nu_0))/((1+nu_0)*(1-2*nu_0));
C(1,1) = const;
C(1,2)= const*(nu_0/(1-nu_0));
C(1,3)= const*(nu_0/(1-nu_0));
C(2,1) = C(1,2);
C(2,2) = const;
C(2,3) = const*(nu_0/(1-nu_0));
C(3,1) = C(1,3);
C(3,2) = C(2,3);
C(3,3) = const;
C(4,4) = const*((1-2*nu_0)/(2*(1-nu_0)));
```

```
C(5,5) = const*((1-2*nu_0)/(2*(1-nu_0)));
C(6,6) = const*((1-2*nu_0)/(2*(1-nu_0)));
C;

% Elastic properties - inclusion
E_i = 386
nu_i = 0.22

D = zeros (6,6);
const = (E_i*(1-nu_i))/((1+nu_i)*(1-2*nu_i));
D(1,1) = const;
D(1,2)= const*(nu_i/(1-nu_i));
D(1,3)= const*(nu_i/(1-nu_i));
D(2,1) = D(1,2);
D(2,2) = const;
D(2,3) = const*(nu_i/(1-nu_i));
D(3,1) = D(1,3);
D(3,2) = D(2,3);
D(3,3) = const;
D(4,4) = const*((1-2*nu_i)/(2*(1-nu_i)));
D(5,5) = const*((1-2*nu_i)/(2*(1-nu_i)));
D(6,6) = const*((1-2*nu_i)/(2*(1-nu_i)));
D;

% Elastic properties  - agglomerates/voids
E_a = 10.0
nu_a = 0.35

F = zeros (6,6);
const = (E_a*(1-nu_a))/((1+nu_a)*(1-2*nu_a));
F(1,1) = const;
F(1,2)= const*(nu_a/(1-nu_a));
F(1,3)= const*(nu_a/(1-nu_a));
F(2,1) = F(1,2);
F(2,2) = const;
F(2,3) = const*(nu_a/(1-nu_a));
F(3,1) = F(1,3);
F(3,2) = F(2,3);
F(3,3) = const;
F(4,4) = const*((1-2*nu_a)/(2*(1-nu_a)));
F(5,5) = const*((1-2*nu_a)/(2*(1-nu_a)));
F(6,6) = const*((1-2*nu_a)/(2*(1-nu_a)));
F;
```

```
% GEOEMTRY SETTINGS
% Geometry - inclusions:
geom_i = 1  % spherical inclusions
%geom_i = 2  % fibre-like inclusions
%geom_i = 3  % disc-shaped inclusions

% Geometry - agglomerates/voids:
geom_a = 1  % spherical inclusions
%geom_a = 2  % fibre-like inclusions
%geom_a = 3  % disc-shaped inclusions

% INCLUSIONS
if (geom_i == 1)
  % Spherical inclusions:
  Si_1111 = (7-5*nu_0)/(15*(1-nu_0));
  Si_2222 = Si_1111;
  Si_3333 = Si_1111;
  Si_1122 = (5*nu_0-1)/(15*(1-nu_0));
  Si_1133 = Si_1122;
  Si_2211 = Si_1122;
  Si_2233 = Si_1122;
  Si_3311 = Si_1122;
  Si_3322 = Si_1122;
  Si_1212 = (4-5*nu_0)/(15*(1-nu_0));
  Si_1221 = Si_1212;
  Si_2323 = Si_1212;
  Si_2332 = Si_1212;
  Si_3131 = Si_1212;
  Si_3113 = Si_1212;

elseif (geom_i == 2)
  % Fiber-like inclusions:
  l = 20       % fibre length
  d = 1       % fibre diameter
  a = l/d     % aspect ratio

  a2 = power(a,2.0)

  g = (a/power(a2-1,1.5))*(a*sqrt(a2-1)-acosh(a))

  b = 1/(1-nu_0)
  c = 1-2*nu_0
  e = 1/(a2-1)
```

```
  Si_1111 = 0.5*b*(c + e*(3*a2-1)-(c+3*e*a2)*g)
  Si_2222 = (3/8)*b*e*a2+0.25*b*(c-(9/4)*e)*g;
  Si_3333 = Si_2222;
  Si_2233 = 0.25*b*(0.5*e*a2-(c+0.75*e)*g);
  Si_3322 = Si_2233;
  Si_2211 = -0.5*b*e*a2 + 0.25*b*(3*e*a2-c)*g;
  Si_3311 = Si_2211;
  Si_1122 = -0.5*b*(c+e)+0.5*b*(c+1.5*e)*g;
  Si_1133 = Si_1122;
  Si_2323 = 0.25*b*(0.5*e*a2 + (c-0.75*e)*g);
  Si_3232 = Si_2323;
  Si_1212 = 0.25*b*(c-(a2+1)*e-0.5*(c-3*e*(a2+1))*g);
  Si_1313 = Si_1212;
  Si_3131 = Si_1313;

elseif (geom_i == 3)
  % Disc-shaped inclusions
  l = 0.5       % fibre length
  d = 1       % fibre diameter
  a = l/d     % aspect ratio
  a2 = power(a,2.0)
  g = (a/power(1-a2,1.5))*(acos(a)-a*sqrt(1-a2))
  b = 1/(1-nu_0)
  c = 1-2*nu_0
  e = 1/(a2-1)

  Si_1111 = 0.5*b*(c + e*(3*a2-1)-(c+3*e*a2)*g);
  Si_2222 = (3/8)*b*e*a2+0.25*b*(c-(9/4)*e)*g;
  Si_3333 = Si_2222;
  Si_2233 = 0.25*b*(0.5*e*a2-(c+0.75*e)*g);
  Si_3322 = Si_2233;
  Si_2211 = -0.5*b*e*a2 + 0.25*b*(3*e*a2-c)*g;
  Si_3311 = Si_2211;
  Si_1122 = -0.5*b*(c+e)+0.5*b*(c+1.5*e)*g;
  Si_1133 = Si_1122;
  Si_2323 = 0.25*b*(0.5*e*a2 + (c-0.75*e)*g);
  Si_3232 = Si_2323;
  Si_1212 = 0.25*b*(c-(a2+1)*e-0.5*(c-3*e*(a2+1))*g);
  Si_1313 = Si_1212;
  Si_3131 = Si_1313;
end

% Eshelby tensor (using engineering strains)
```

```
Si = zeros(6,6);
% Matrix form:
Si(1,1) = Si_1111;
Si(1,2) = Si_1122;
Si(1,3) = Si_1133;
Si(2,1) = Si_2211;
Si(2,2) = Si_2222;
Si(2,3) = Si_2233;
Si(3,1) = Si_3311;
Si(3,2) = Si_3322;
Si(3,3) = Si_3333;
Si(4,4) = 2*Si_1212;
Si(5,5) = 2*Si_2323;
Si(6,6) = 2*Si_3131;
Si;

% AGGLOMERATES/VOIDS
if (geom_a == 1)
  % Spherical agglomerates/voids:
  Sa_1111 = (7-5*nu_0)/(15*(1-nu_0));
  Sa_2222 = Sa_1111;
  Sa_3333 = Sa_1111;
  Sa_1122 = (5*nu_0-1)/(15*(1-nu_0));
  Sa_1133 = Sa_1122;
  Sa_2211 = Sa_1122;
  Sa_2233 = Sa_1122;
  Sa_3311 = Sa_1122;
  Sa_3322 = Sa_1122;
  Sa_1212 = (4-5*nu_0)/(15*(1-nu_0));
  Sa_1221 = Sa_1212;
  Sa_2323 = Sa_1212;
  Sa_2332 = Sa_1212;
  Sa_3131 = Sa_1212;
  Sa_3113 = Sa_1212;

elseif (geom_a == 2)
  % Fiber-like agglomerates/voids:
  l = 20       % fibre length
  d = 1       % fibre diameter
  a = l/d     % aspect ratio
  a2 = power(a,2.0)
  g = (a/power(a2-1,1.5))*(a*sqrt(a2-1)-acosh(a))
  b = 1/(1-nu_0)
```

```
  c = 1-2*nu_0
  e = 1/(a2-1)

  Sa_1111 = 0.5*b*(c + e*(3*a2-1)-(c+3*e*a2)*g)
  Sa_2222 = (3/8)*b*e*a2+0.25*b*(c-(9/4)*e)*g;
  Sa_3333 = Sa_2222;
  Sa_2233 = 0.25*b*(0.5*e*a2-(c+0.75*e)*g);
  Sa_3322 = Sa_2233;
  Sa_2211 = -0.5*b*e*a2 + 0.25*b*(3*e*a2-c)*g;
  Sa_3311 = Sa_2211;
  Sa_1122 = -0.5*b*(c+e)+0.5*b*(c+1.5*e)*g;
  Sa_1133 = Sa_1122;
  Sa_2323 = 0.25*b*(0.5*e*a2 + (c-0.75*e)*g);
  Sa_3232 = Sa_2323;
  Sa_1212 = 0.25*b*(c-(a2+1)*e-0.5*(c-3*e*(a2+1))*g);
  Sa_1313 = Sa_1212;
  Sa_3131 = Sa_1313;

elseif (geom_a == 3)
  % Disc-shaped agglomerates/voids:
  l = 0.5       % fibre length
  d = 1       % fibre diameter
  a = l/d     % aspect ratio
  a2 = power(a,2.0)

  g = (a/power(1-a2,1.5))*(acos(a)-a*sqrt(1-a2))
  b = 1/(1-nu_0)
  c = 1-2*nu_0
  e = 1/(a2-1)

  Sa_1111 = 0.5*b*(c + e*(3*a2-1)-(c+3*e*a2)*g);
  Sa_2222 = (3/8)*b*e*a2+0.25*b*(c-(9/4)*e)*g;
  Sa_3333 = Sa_2222;
  Sa_2233 = 0.25*b*(0.5*e*a2-(c+0.75*e)*g);
  Sa_3322 = Sa_2233;
  Sa_2211 = -0.5*b*e*a2 + 0.25*b*(3*e*a2-c)*g;
  Sa_3311 = Sa_2211;
  Sa_1122 = -0.5*b*(c+e)+0.5*b*(c+1.5*e)*g;
  Sa_1133 = Sa_1122;
  Sa_2323 = 0.25*b*(0.5*e*a2 + (c-0.75*e)*g);
  Sa_3232 = Sa_2323;
  Sa_1212 = 0.25*b*(c-(a2+1)*e-0.5*(c-3*e*(a2+1))*g);
  Sa_1313 = Sa_1212;
```

```
  Sa_3131 = Sa_1313;
end

% Eshelby tensor (using engineering strains)
Sa = zeros(6,6);
% Matrix form:
Sa(1,1) = Sa_1111;
Sa(1,2) = Sa_1122;
Sa(1,3) = Sa_1133;
Sa(2,1) = Sa_2211;
Sa(2,2) = Sa_2222;
Sa(2,3) = Sa_2233;
Sa(3,1) = Sa_3311;
Sa(3,2) = Sa_3322;
Sa(3,3) = Sa_3333;
Sa(4,4) = 2*Sa_1212;
Sa(5,5) = 2*Sa_2323;
Sa(6,6) = 2*Sa_3131;
Sa;

% CALCULATIONS
% Dilute matrix
I = zeros(6,6);
I(1,1) = 1.0;
I(2,2) = 1.0;
I(3,3) = 1.0;
I(4,4) = 1.0;
I(5,5) = 1.0;
I(6,6) = 1.0;
I;

Ai_dil = inv(I+Si*inv(C)*(D-C))
Aa_dil = inv(I+Sa*inv(C)*(F-C))

Va =0.01

for j = 1:length(Va)
  Vf = 0.0:0.001:0.2;
  for i =1:length(Vf)
    V0 =(1-Va(j)-Vf(i));
    A_0 = inv(V0*I + Vf(i)*Ai_dil + Va(j)*Aa_dil);
    Ai_r = Ai_dil*A_0;
    Aa_r = Aa_dil*A_0;
```

```
    C_comp = V0*C*A_0 + Vf(i)*D*Ai_r + Va(j)*F*Aa_r

    % Transversely isotropic proerties
    S_comp = inv(C_comp);
    E_11(j,i) = 1/(S_comp(1,1)*E_0);
    %end
  end

  plot(Vf,E_11,'k')
  hold on
end

% PLOTTING
xlabel ('V_f')
ylabel('E_{comp}/E_m')
```

B.4 General three-phase Mori-Tanaka model for randomly oriented inclusions

```
% General Mori-Tanaka three-phase model
% This case: Two types of isotropic inclusions
% Three geometries:
% 1) random spherical inclusions
% 2) random fibre-like inclusions with aspect ratio
% 3) random disc-shaped inclusion with aspect ratio
%
% Author: Tom Thorvaldsen, FFI, March 2014

% MATERIAL PARAMETERS
% Elastic properties - matrix
E_0 = 3.12
nu_0 = 0.35

C = zeros (6,6);
const = (E_0*(1-nu_0))/((1+nu_0)*(1-2*nu_0));
C(1,1) = const;
C(1,2)= const*(nu_0/(1-nu_0));
C(1,3)= const*(nu_0/(1-nu_0));
C(2,1) = C(1,2);
C(2,2) = const;
C(2,3) = const*(nu_0/(1-nu_0));
C(3,1) = C(1,3);
C(3,2) = C(2,3);
C(3,3) = const;
C(4,4) = const*((1-2*nu_0)/(2*(1-nu_0)));
```

```
C(5,5) = const*((1-2*nu_0)/(2*(1-nu_0)));
C(6,6) = const*((1-2*nu_0)/(2*(1-nu_0)));
C;

% Elastic properties - inclusion
E_i = 386
nu_i = 0.35

D = zeros (6,6);
const = (E_i*(1-nu_i))/((1+nu_i)*(1-2*nu_i));
D(1,1) = const;
D(1,2)= const*(nu_i/(1-nu_i));
D(1,3)= const*(nu_i/(1-nu_i));
D(2,1) = D(1,2);
D(2,2) = const;
D(2,3) = const*(nu_i/(1-nu_i));
D(3,1) = D(1,3);
D(3,2) = D(2,3);
D(3,3) = const;
D(4,4) = const*((1-2*nu_i)/(2*(1-nu_i)));
D(5,5) = const*((1-2*nu_i)/(2*(1-nu_i)));
D(6,6) = const*((1-2*nu_i)/(2*(1-nu_i)));
D;

% Elastic properties - agglomerates/voids
E_a = 0.0
nu_a = 0.35

F = zeros (6,6);
const = (E_a*(1-nu_a))/((1+nu_a)*(1-2*nu_a));
F(1,1) = const;
F(1,2)= const*(nu_a/(1-nu_a));
F(1,3)= const*(nu_a/(1-nu_a));
F(2,1) = F(1,2);
F(2,2) = const;
F(2,3) = const*(nu_a/(1-nu_a));
F(3,1) = F(1,3);
F(3,2) = F(2,3);
F(3,3) = const;
F(4,4) = const*((1-2*nu_a)/(2*(1-nu_a)));
F(5,5) = const*((1-2*nu_a)/(2*(1-nu_a)));
F(6,6) = const*((1-2*nu_a)/(2*(1-nu_a)));
F;
```

```
% GEOEMTRY SETTINGS
% Geometry - inclusions:
%geom_i = 1  % spherical inclusions
geom_i = 2  % fibre-like inclusions
%geom_i = 3  % disc-shaped inclusions

% Geometry - agglomerates/voids:
geom_a = 1  % spherical inclusions
%geom_a = 2  % fibre-like inclusions; NOT FULLY SUPPORTED
%geom_a = 3  % disc-shaped inclusions; NOT FULLY SUPPORTED

% INCLUSIONS
if (geom_i == 1)
  % Spherical inclusions:
  Si_1111 = (7-5*nu_0)/(15*(1-nu_0));
  Si_2222 = Si_1111;
  Si_3333 = Si_1111;
  Si_1122 = (5*nu_0-1)/(15*(1-nu_0));
  Si_1133 = Si_1122;
  Si_2211 = Si_1122;
  Si_2233 = Si_1122;
  Si_3311 = Si_1122;
  Si_3322 = Si_1122;
  Si_1212 = (4-5*nu_0)/(15*(1-nu_0));
  Si_1221 = Si_1212;
  Si_2323 = Si_1212;
  Si_2332 = Si_1212;
  Si_3131 = Si_1212;
  Si_3113 = Si_1212;

elseif (geom_i == 2)
  % Fiber-like inclusions:
  l = 20       % fibre length
  d = 1       % fibre diameter
  a = l/d     % aspect ratio
  a2 = power(a,2.0)
  g = (a/power(a2-1,1.5))*(a*sqrt(a2-1)-acosh(a))
  b = 1/(1-nu_0)
  c = 1-2*nu_0
  e = 1/(a2-1)

  Si_1111 = 0.5*b*(c + e*(3*a2-1)-(c+3*e*a2)*g)
  Si_2222 = (3/8)*b*e*a2+0.25*b*(c-(9/4)*e)*g;
```

```
  Si_3333 = Si_2222;
  Si_2233 = 0.25*b*(0.5*e*a2-(c+0.75*e)*g);
  Si_3322 = Si_2233;
  Si_2211 = -0.5*b*e*a2 + 0.25*b*(3*e*a2-c)*g;
  Si_3311 = Si_2211;
  Si_1122 = -0.5*b*(c+e)+0.5*b*(c+1.5*e)*g;
  Si_1133 = Si_1122;
  Si_2323 = 0.25*b*(0.5*e*a2 + (c-0.75*e)*g);
  Si_3232 = Si_2323;
  Si_1212 = 0.25*b*(c-(a2+1)*e-0.5*(c-3*e*(a2+1))*g);
  Si_1313 = Si_1212;
  Si_3131 = Si_1313;

elseif (geom_i == 3)
  % Disc-shaped inclusions
  l = 0.5       % fibre length
  d = 1       % fibre diameter
  a = l/d     % aspect ratio
  a2 = power(a,2.0)
  g = (a/power(1-a2,1.5))*(acos(a)-a*sqrt(1-a2))
  b = 1/(1-nu_0)
  c = 1-2*nu_0
  e = 1/(a2-1)

  Si_1111 = 0.5*b*(c + e*(3*a2-1)-(c+3*e*a2)*g);
  Si_2222 = (3/8)*b*e*a2+0.25*b*(c-(9/4)*e)*g;
  Si_3333 = Si_2222;
  Si_2233 = 0.25*b*(0.5*e*a2-(c+0.75*e)*g);
  Si_3322 = Si_2233;
  Si_2211 = -0.5*b*e*a2 + 0.25*b*(3*e*a2-c)*g;
  Si_3311 = Si_2211;
  Si_1122 = -0.5*b*(c+e)+0.5*b*(c+1.5*e)*g;
  Si_1133 = Si_1122;
  Si_2323 = 0.25*b*(0.5*e*a2 + (c-0.75*e)*g);
  Si_3232 = Si_2323;
  Si_1212 = 0.25*b*(c-(a2+1)*e-0.5*(c-3*e*(a2+1))*g);
  Si_1313 = Si_1212;
  Si_3131 = Si_1313;
end

% Eshelby tensor (using engineering strains)
Si = zeros(6,6);
```

```
% Matrix form:
Si(1,1) = Si_1111;
Si(1,2) = Si_1122;
Si(1,3) = Si_1133;
Si(2,1) = Si_2211;
Si(2,2) = Si_2222;
Si(2,3) = Si_2233;
Si(3,1) = Si_3311;
Si(3,2) = Si_3322;
Si(3,3) = Si_3333;
Si(4,4) = 2*Si_1212;
Si(5,5) = 2*Si_2323;
Si(6,6) = 2*Si_3131;
Si;

% AGGLOMERATES/VOIDS
if (geom_a == 1)
  % Spherical agglomerates/voids:
  Sa_1111 = (7-5*nu_0)/(15*(1-nu_0));
  Sa_2222 = Sa_1111;
  Sa_3333 = Sa_1111;
  Sa_1122 = (5*nu_0-1)/(15*(1-nu_0));
  Sa_1133 = Sa_1122;
  Sa_2211 = Sa_1122;
  Sa_2233 = Sa_1122;
  Sa_3311 = Sa_1122;
  Sa_3322 = Sa_1122;
  Sa_1212 = (4-5*nu_0)/(15*(1-nu_0));
  Sa_1221 = Sa_1212;
  Sa_2323 = Sa_1212;
  Sa_2332 = Sa_1212;
  Sa_3131 = Sa_1212;
  Sa_3113 = Sa_1212;
elseif (geom_a == 2)
  % Fiber-like agglomerates/voids:
  l = 20       % fibre length
  d = 1       % fibre diameter
  a = l/d     % aspect ratio
  a2 = power(a,2.0)

  g = (a/power(a2-1,1.5))*(a*sqrt(a2-1)-acosh(a))
  b = 1/(1-nu_0)
  c = 1-2*nu_0
```

```
  e = 1/(a2-1)

  Sa_1111 = 0.5*b*(c + e*(3*a2-1)-(c+3*e*a2)*g)
  Sa_2222 = (3/8)*b*e*a2+0.25*b*(c-(9/4)*e)*g;
  Sa_3333 = Sa_2222;
  Sa_2233 = 0.25*b*(0.5*e*a2-(c+0.75*e)*g);
  Sa_3322 = Sa_2233;
  Sa_2211 = -0.5*b*e*a2 + 0.25*b*(3*e*a2-c)*g;
  Sa_3311 = Sa_2211;
  Sa_1122 = -0.5*b*(c+e)+0.5*b*(c+1.5*e)*g;
  Sa_1133 = Sa_1122;
  Sa_2323 = 0.25*b*(0.5*e*a2 + (c-0.75*e)*g);
  Sa_3232 = Sa_2323;
  Sa_1212 = 0.25*b*(c-(a2+1)*e-0.5*(c-3*e*(a2+1))*g);
  Sa_1313 = Sa_1212;
  Sa_3131 = Sa_1313;
elseif (geom_a == 3)
  % Disc-shaped agglomerates/voids:
  l = 0.5       % fibre length
  d = 1       % fibre diameter
  a = l/d     % aspect ratio
  a2 = power(a,2.0)
  g = (a/power(1-a2,1.5))*(acos(a)-a*sqrt(1-a2))
  b = 1/(1-nu_0)
  c = 1-2*nu_0
  e = 1/(a2-1)

  Sa_1111 = 0.5*b*(c + e*(3*a2-1)-(c+3*e*a2)*g);
  Sa_2222 = (3/8)*b*e*a2+0.25*b*(c-(9/4)*e)*g;
  Sa_3333 = Sa_2222;
  Sa_2233 = 0.25*b*(0.5*e*a2-(c+0.75*e)*g);
  Sa_3322 = Sa_2233;
  Sa_2211 = -0.5*b*e*a2 + 0.25*b*(3*e*a2-c)*g;
  Sa_3311 = Sa_2211;
  Sa_1122 = -0.5*b*(c+e)+0.5*b*(c+1.5*e)*g;
  Sa_1133 = Sa_1122;
  Sa_2323 = 0.25*b*(0.5*e*a2 + (c-0.75*e)*g);
  Sa_3232 = Sa_2323;
  Sa_1212 = 0.25*b*(c-(a2+1)*e-0.5*(c-3*e*(a2+1))*g);
  Sa_1313 = Sa_1212;
  Sa_3131 = Sa_1313;
end
```

```
% Eshelby tensor (using engineering strains)
Sa = zeros(6,6);

% Matrix form:
Sa(1,1) = Sa_1111;
Sa(1,2) = Sa_1122;
Sa(1,3) = Sa_1133;
Sa(2,1) = Sa_2211;
Sa(2,2) = Sa_2222;
Sa(2,3) = Sa_2233;
Sa(3,1) = Sa_3311;
Sa(3,2) = Sa_3322;
Sa(3,3) = Sa_3333;
Sa(4,4) = 2*Sa_1212;
Sa(5,5) = 2*Sa_2323;
Sa(6,6) = 2*Sa_3131;
Sa;

% CALCULATIONS
% Dilute matrix
I = zeros(6,6);
I(1,1) = 1.0;
I(2,2) = 1.0;
I(3,3) = 1.0;
I(4,4) = 1.0;
I(5,5) = 1.0;
I(6,6) = 1.0;
I;

Ai_dil = inv(I+Si*inv(C)*(D-C))
Aa_dil = inv(I+Sa*inv(C)*(F-C))

% Random average matrix
M =(1/120)*[24 64 0 16 16 0 0 0 0 0 0 64;
  24 9 45 6 6 10 10 5 5 20 40 24;
  24 9 45 6 6 10 10 5 5 20 40 24;
  8 8 0 12 32 20 0 40 0 0 0 -32;
  8 8 0 32 12 0 20 0 40 0 0 -32;
  8 8 0 12 32 20 0 40 0 0 0 -32;
  8 8 0 32 12 0 20 0 40 0 0 -32;
  8 3 15 2 2 30 30 15 15 -20 -40 8;
  8 3 15 2 2 30 30 15 15 -20 -40 8;
  8 3 15 2 2 -10 -10 -5 -5 20 40 8;
```

```
  8 8 0 -8 -8 0 0 0 0 40 20 28;
  8 8 0 -8 -8 0 0 0 0 40 20 28]

% AVERAGING OF THE FIRST INCLUSION PHASE
D_Ai_dil = D*Ai_dil

% Averaging of D_Ai_dil
D_Ai_dil_vec(1) = D_Ai_dil(1,1);
D_Ai_dil_vec(2) = D_Ai_dil(2,2);
D_Ai_dil_vec(3) = D_Ai_dil(3,3);
D_Ai_dil_vec(4) = D_Ai_dil(1,2);
D_Ai_dil_vec(5) = D_Ai_dil(2,1);
D_Ai_dil_vec(6) = D_Ai_dil(1,3);
D_Ai_dil_vec(7) = D_Ai_dil(3,1);
D_Ai_dil_vec(8) = D_Ai_dil(2,3);
D_Ai_dil_vec(9) = D_Ai_dil(3,2);
D_Ai_dil_vec(10) = D_Ai_dil(4,4);
D_Ai_dil_vec(11) = D_Ai_dil(5,5);
D_Ai_dil_vec(12) = D_Ai_dil(6,6);

D_Ai_dil_aver_vec = M*transpose(D_Ai_dil_vec);

D_Ai_dil_aver(1,1) = D_Ai_dil_aver_vec(1);
D_Ai_dil_aver(2,2) = D_Ai_dil_aver_vec(2);
D_Ai_dil_aver(3,3) = D_Ai_dil_aver_vec(3);
D_Ai_dil_aver(1,2) = D_Ai_dil_aver_vec(4);
D_Ai_dil_aver(2,1) = D_Ai_dil_aver_vec(5);
D_Ai_dil_aver(1,3) = D_Ai_dil_aver_vec(6);
D_Ai_dil_aver(3,1) = D_Ai_dil_aver_vec(7);
D_Ai_dil_aver(2,3) = D_Ai_dil_aver_vec(8);
D_Ai_dil_aver(3,2) = D_Ai_dil_aver_vec(9);
D_Ai_dil_aver(4,4) = D_Ai_dil_aver_vec(10);
D_Ai_dil_aver(5,5) = D_Ai_dil_aver_vec(11);
D_Ai_dil_aver(6,6) = D_Ai_dil_aver_vec(12);
D_Ai_dil_aver;

% Averaging of Ai_dil
Ai_dil_vec(1) = Ai_dil(1,1);
Ai_dil_vec(2) = Ai_dil(2,2);
Ai_dil_vec(3) = Ai_dil(3,3);
Ai_dil_vec(4) = Ai_dil(1,2);
Ai_dil_vec(5) = Ai_dil(2,1);
Ai_dil_vec(6) = Ai_dil(1,3);
```

```
Ai_dil_vec(7) = Ai_dil(3,1);
Ai_dil_vec(8) = Ai_dil(2,3);
Ai_dil_vec(9) = Ai_dil(3,2);
Ai_dil_vec(10) = Ai_dil(4,4);
Ai_dil_vec(11) = Ai_dil(5,5);
Ai_dil_vec(12) = Ai_dil(6,6);

Ai_dil_aver_vec = M*transpose(Ai_dil_vec);

Ai_dil_aver(1,1) = Ai_dil_aver_vec(1);
Ai_dil_aver(2,2) = Ai_dil_aver_vec(2);
Ai_dil_aver(3,3) = Ai_dil_aver_vec(3);
Ai_dil_aver(1,2) = Ai_dil_aver_vec(4);
Ai_dil_aver(2,1) = Ai_dil_aver_vec(5);
Ai_dil_aver(1,3) = Ai_dil_aver_vec(6);
Ai_dil_aver(3,1) = Ai_dil_aver_vec(7);
Ai_dil_aver(2,3) = Ai_dil_aver_vec(8);
Ai_dil_aver(3,2) = Ai_dil_aver_vec(9);
Ai_dil_aver(4,4) = Ai_dil_aver_vec(10);
Ai_dil_aver(5,5) = Ai_dil_aver_vec(11);
Ai_dil_aver(6,6) = Ai_dil_aver_vec(12);
Ai_dil_aver;

% AVERAGING OF THE SECOND INCLUSION PHASE (agglomerates/voids)
F_Aa_dil = F*Aa_dil

% Averaging of F_Aa_dil
F_Aa_dil_vec(1) = F_Aa_dil(1,1);
F_Aa_dil_vec(2) = F_Aa_dil(2,2);
F_Aa_dil_vec(3) = F_Aa_dil(3,3);
F_Aa_dil_vec(4) = F_Aa_dil(1,2);
F_Aa_dil_vec(5) = F_Aa_dil(2,1);
F_Aa_dil_vec(6) = F_Aa_dil(1,3);
F_Aa_dil_vec(7) = F_Aa_dil(3,1);
F_Aa_dil_vec(8) = F_Aa_dil(2,3);
F_Aa_dil_vec(9) = F_Aa_dil(3,2);
F_Aa_dil_vec(10) = F_Aa_dil(4,4);
F_Aa_dil_vec(11) = F_Aa_dil(5,5);
F_Aa_dil_vec(12) = F_Aa_dil(6,6);

F_Aa_dil_aver_vec = M*transpose(F_Aa_dil_vec);

F_Aa_dil_aver(1,1) = F_Aa_dil_aver_vec(1);
```

```
F_Aa_dil_aver(2,2) = F_Aa_dil_aver_vec(2);
F_Aa_dil_aver(3,3) = F_Aa_dil_aver_vec(3);
F_Aa_dil_aver(1,2) = F_Aa_dil_aver_vec(4);
F_Aa_dil_aver(2,1) = F_Aa_dil_aver_vec(5);
F_Aa_dil_aver(1,3) = F_Aa_dil_aver_vec(6);
F_Aa_dil_aver(3,1) = F_Aa_dil_aver_vec(7);
F_Aa_dil_aver(2,3) = F_Aa_dil_aver_vec(8);
F_Aa_dil_aver(3,2) = F_Aa_dil_aver_vec(9);
F_Aa_dil_aver(4,4) = F_Aa_dil_aver_vec(10);
F_Aa_dil_aver(5,5) = F_Aa_dil_aver_vec(11);
F_Aa_dil_aver(6,6) = F_Aa_dil_aver_vec(12);
F_Aa_dil_aver;

% Averaging of Aa_dil
Aa_dil_vec(1) = Aa_dil(1,1);
Aa_dil_vec(2) = Aa_dil(2,2);
Aa_dil_vec(3) = Aa_dil(3,3);
Aa_dil_vec(4) = Aa_dil(1,2);
Aa_dil_vec(5) = Aa_dil(2,1);
Aa_dil_vec(6) = Aa_dil(1,3);
Aa_dil_vec(7) = Aa_dil(3,1);
Aa_dil_vec(8) = Aa_dil(2,3);
Aa_dil_vec(9) = Aa_dil(3,2);
Aa_dil_vec(10) = Aa_dil(4,4);
Aa_dil_vec(11) = Aa_dil(5,5);
Aa_dil_vec(12) = Aa_dil(6,6);

Aa_dil_aver_vec = M*transpose(Aa_dil_vec);

Aa_dil_aver(1,1) = Aa_dil_aver_vec(1);
Aa_dil_aver(2,2) = Aa_dil_aver_vec(2);
Aa_dil_aver(3,3) = Aa_dil_aver_vec(3);
Aa_dil_aver(1,2) = Aa_dil_aver_vec(4);
Aa_dil_aver(2,1) = Aa_dil_aver_vec(5);
Aa_dil_aver(1,3) = Aa_dil_aver_vec(6);
Aa_dil_aver(3,1) = Aa_dil_aver_vec(7);
Aa_dil_aver(2,3) = Aa_dil_aver_vec(8);
Aa_dil_aver(3,2) = Aa_dil_aver_vec(9);
Aa_dil_aver(4,4) = Aa_dil_aver_vec(10);
Aa_dil_aver(5,5) = Aa_dil_aver_vec(11);
Aa_dil_aver(6,6) = Aa_dil_aver_vec(12);
Aa_dil_aver;
```

```
% CALCULATIONS
Va =0.05
Vf = 0.0:0.001:0.018;

for i =1:length(Vf)
  V0 =(1-Va-Vf(i));

  % NOTE: Current version only support SPHERICAL SHAPED
AGLOMERATES/VOIDS
  if (geom_i == 1 & geom_a == 1)
    %Gives the correct spherical distr.
    A_0 = inv(V0*I + Vf(i)*Ai_dil + Va*Aa_dil);
  elseif (geom_i == 2 & geom_a == 1)
    % gives a transversely iso C_comp
    A_0 = inv(V0*I + Vf(i)*Ai_dil_aver + Va*Aa_dil);
  elseif (geom_i == 3 & geom_a == 1)
    A_0 = inv(V0*I + Vf(i)*Ai_dil_aver + Va*Aa_dil);
    % Additional elseif statements needed in case aglomerates/voids
    % have a different geometry
  end

  C_comp = (V0*C + Vf(i)*D_Ai_dil_aver + Va*F_Aa_dil_aver)*A_0

  % Transversely isotropic properties
  S_comp = inv(C_comp);
  E_11(i) = 1/(S_comp(1,1)*E_0);
end

% PLOTTING
plot(Vf,E_11,'m')
hold on
xlabel ('V_f')
ylabel('E_{comp}/E_0')
```

B.5 Weng three-phase model

```
% Weng three-phase model
% This case: Two types of isotropic inclusions (three-phase model)
% Geometry: random spherical inclusions
% Refererence: Weng, 1984
%
% Author: Tom Thorvaldsen, FFI, March 2014

% Elastic properties - matrix
```

```
E_0 = 3.12
nu_0 =  0.35
mu_0 = E_0/(2*(1+nu_0))
kappa_0 = E_0/(3*(1-2*nu_0))
alpha_0 = (3*kappa_0)/(3*kappa_0+4*mu_0)
beta_0 = (6/5)*((kappa_0+2*mu_0)/(3*kappa_0+4*mu_0))

% Elastic properties - inclusion (phase 1)
E_f =  386
nu_f = 0.22
mu_f = E_f/(2*(1+nu_f))
kappa_f = E_f/(3*(1-2*nu_f))

% Elastic properties - agglomerates/voids (phase 2)
E_a =  3.12 % GPa
nu_a = 0.35 %
mu_a = E_a/(2*(1+nu_a))
kappa_a = E_a/(3*(1-2*nu_a))

V_f = 0.0:0.001:0.2;
V_a = 0.01

for i =1:length(V_f)
  a=(V_f(i)*(kappa_f-kappa_0))/(alpha_0*(kappa_f-kappa_0)+kappa_0)...
      +(V_a*(kappa_a-kappa_0))/(alpha_0*(kappa_a-kappa_0)+kappa_0)

  b=(V_f(i)*(mu_f-mu_0))/(beta_0*(mu_f-mu_0)+mu_0)...
      +(V_a*(mu_a-mu_0))/(beta_0*(mu_a-mu_0)+mu_0)

  kappa_c(i)=1+a/(1-alpha_0*a)
  mu_c(i)=1+b/(1-beta_0*b)

  % Effective Young's modulus (normalized)
  E_c(i)= kappa_c(i)*mu_c(i)*(3*kappa_0+mu_0)/...
      (3*kappa_c(i)*kappa_0+mu_c(i)*mu_0);
end

plot(V_f,E_c, 'g')
xlabel ('V_f')
ylabel('E_{comp}/E_m')
legend('E_a=0 (voids)', 'E_a=1 GPa', 'E_a=E_m', 'E_a= 10 GPa')
```

B.6 Cohen-Ishai three-phase model

```
% Cohen and Ishai three-phase model
% This case: One type of isotropic inclusions and voids
% References: Cohen and Ishai, 1967
%
% Author: Tom Thorvaldsen, FFI, March 2014

% Stiffness - matrix
E_m = 3.12
nu_m = 0.35

% Stiffness - inclusion
E_f = 386
nu_f = 0.22

V_f = 0.0:0.001:0.015
V_a = 0.005

for i = 1:length(V_f)
  E_cv = E_m*(1-power(V_a,2/3))
  m = E_f/E_cv
  E_comp = E_cv*(1+(V_f(i)/((m/(m-1))-nthroot(V_f(i),3))))
  E_11(i) = E_comp/E_m;
end

plot(V_f,E_11,'k--')
xlabel ('V_f')
ylabel('E_{comp}/E_0')
```

B.7 Paul three-phase model

```
% Paul three-phase model
% This case: One type of isotropic inclusions and voids
% References: Paul, 1967
%
% Author: Tom Thorvaldsen, FFI, March 2014

% Stiffness - matrix
E_m = 3.12 %GPa % 2.76 %GPa
nu_m = 0.35;

% Stiffness - inclusion
E_f = 386.0 % GPa % 72.4;
```

```
nu_f = 0.22  %0.2;

V_f = 0.0:0.001:0.015
V_a = 0.005

for i = 1:length(V_f)
  E_cv = E_m*((1-power(V_a,2/3))/(1-power(V_a,2/3)+V_a))
  m = E_f/E_cv
  E_comp = E_cv*((1+(m-1)*power(V_f(i),2/3))/(1+(m-
1)*(power(V_f(i),2/3)-V_f(i))))
  E_11(i) = E_comp/E_m;
end

plot(V_f,E_11,'c--')
xlabel ('V_f')
ylabel('E_{comp}/E_0')
```

B.8 Cohen-Ishai-Thorvaldsen three-phase model

```
% Cohen-Ishai-Thorvaldsen three-phase model
% This case: One type of isotropic inclusions and agglomerates
% References: Cohen and Ishai, 1967 + Thorvaldsen
%
% Author: Tom Thorvaldsen, FFI,  March 2014

% Elastic properties - matrix
E_m = 3.12
nu_m = 0.35

% Elastic properties - inclusion
E_f = 386
nu_f = 0.22

% Elastic properties- agglomerates
E_a = 1.0
nu_a = 0.35

V_f = 0.0:0.001:0.015
V_a = 0.005

for i = 1:length(V_f)
  m_a = E_a/E_m
  E_ca = E_m*(1+(V_a/((m_a/(m_a-1))-nthroot(V_a,3))))
```

```
  m = E_f/E_ca
  E_comp = E_ca*(1+(V_f(i)/((m/(m-1))-nthroot(V_f(i),3))))
  E_11(i) = E_comp/E_m;
end

plot(V_f,E_11,'k')
xlabel ('V_f')
ylabel('E_{comp}/E_0')
```

B.9 Paul-Thorvaldsen three-phase model

```
% Paul-Thorvaldsen three-phase model
% This case: One type of isotropic inclusions and agglomerates
% References: Paul, 1967 + Thorvaldsen
%
% Author: Tom Thorvaldsen, FFI, January 2014

% Elastic properties - matrix
E_m = 3.12
nu_m = 0.35

% Elastic properties - inclusion
E_f = 386
nu_f = 0.22

% Elastic properties - agglomerates
E_a = 1.0
nu_a = 0.35

V_f = 0.0:0.001:0.015
V_a = 0.005

for i = 1:length(V_f)
  m_a = E_a/E_m
  E_ca = E_m*((1+(m_a-1)*power(V_a,2/3))/(1+(m_a-1)*(power(V_a,2/3)-
V_a)))

  m = E_f/E_ca
  E_comp = E_ca*((1+(m-1)*power(V_f(i),2/3))/(1+(m-
1)*(power(V_f(i),2/3)-V_f(i))))
  E_11(i) = E_comp/E_m;
end

plot(V_f,E_11,'c')
```

```
xlabel ('V_f')
ylabel('E_{comp}/E_0')
```

References

[1] T. Thorvaldsen, "Modelling the elastic stiffness of nanocomposites using the Mori-Tanaka method ," Forsvarets forskningsinstitutt, FFI report 2015/00494 (Ugradert), 2015.

[2] T. Thorvaldsen, T. R. Frømyr, H. Osnes, and B. B. Johnsen, "A three-phase rule of mixtures model for the effective elastic properties of the combination of dispersed and agglomerated multi-wall carbon nanotubes in a polymer matrix," *Proceedings of the "15th European Conference on Composite Materials"*, 2012.

[3] M. L. Dunn and H. Ledbetter, "Elastic moduli of composites reinforced by multiphase particles," *Journal of Applied Mechanics*, vol. 62, no. 4, pp. 1023-1028, 1995.

[4] B. B. Johnsen, T. R. Frømyr, T. Thorvaldsen, and T. Olsen, "Preparation and characterisation of epoxy/alumina polymer nanocomposites," *Composite Interfaces*, vol. 20, no. 9, pp. 721-740, 2013.

[5] T. Thorvaldsen, B. B. Johnsen, and H. Osnes, "Modelling of nanofibre composites," *Proceedings of the "14th European Conference on Composite Materials"*, 2010.

[6] T. Thorvaldsen, "A model study of the effective Young's modulus for randomly distributed short-fiber composites," FFI report 2011/00212 (Ugradert), 2011.

[7] G. J. Weng, "Some elastic properties of reinforced solids, with special reference to isotropic ones containing spherical inclusions," *International Journal of Enginering Science*, vol. 22, no. 7, pp. 845-856, 1984.

[8] L. J. Cohen and O. Ishai, "The elastic properties of three-phase composites," *Journal of Composite Materials*, vol. 1, no. 4, pp. 390-403, 1967.

[9] O. Ishai and L. J. Cohen, "Elastic properties of filled and porous epoxy composites," *International Journal of Mechanical Sciences*, vol. 9, no. 8, pp. 539-546, 1967.

[10] B. Paul, "Prediction of elastic constants of multi-phase materials," *Transactions of the Metallurgical Society of AIME*, vol. 218, pp. 36-41, 1960.

[11] B. B. Johnsen, A. J. Kinloch, R. D. Mohammed, A. C. Taylor, and S. Sprenger, "Toughening mechanisms of nanoparticle-modified epoxy polymers," *Polymer*, vol. 48, no. 2, pp. 530-541, 2007.

[12] G. P. Tandon and G. J. Weng, "The effect of aspect ratio of inclusions on the elastic properties of unidirectionally aligned composites," *Polymer Composites*, vol. 5, no. 4, pp. 327-333, 1984.

[13] G. P. Tandon and G. J. Weng, "Average stress in the matrix and effective moduli of randomly oriented composites," *Composites Science and Technology*, vol. 27, no. 2, pp. 111-132, 1986.

[14] F. Fisher and L. C. Brinson, "Nanomechanics of nanoreinforced polymers," in *Handbook of theoretical and computational nanotechnology: Functional nanomaterials, nanoparticles, and polymer design*. M. Rieth and W. Schommers, Eds. American Scientific Publishers, 2006, pp. 253-360.